

---

# Accelerating Chain-of-Thought Reasoning: When Goal-Gradient Importance Meets Dynamic Skipping

---

Ren Zhuang, Ben Wang, Shuifa Sun

## Abstract

Large Language Models leverage Chain-of-Thought (CoT) prompting for complex tasks, but their reasoning traces are often excessively verbose and inefficient, leading to significant computational costs and latency. Current CoT compression techniques typically rely on generic importance metrics and static compression rates, which may inadvertently remove functionally critical tokens or fail to adapt to varying reasoning complexity. To overcome these limitations, we propose Adaptive GoGI-Skip, a novel framework learning dynamic CoT compression via supervised fine-tuning. This approach introduces two synergistic innovations: (1) Goal-Gradient Importance (GoGI), a novel metric accurately identifying functionally relevant tokens by measuring the gradient influence of their intermediate representations on the final answer loss, and (2) Adaptive Dynamic Skipping (ADS), a mechanism dynamically regulating the compression rate based on runtime model uncertainty while ensuring local coherence through an adaptive N-token constraint. To our knowledge, this is the first work unifying a goal-oriented, gradient-based importance metric with dynamic, uncertainty-aware skipping for CoT compression. Trained on compressed MATH data, Adaptive GoGI-Skip demonstrates strong cross-domain generalization across diverse reasoning benchmarks including AIME, GPQA, and GSM8K. It achieves substantial efficiency gains—reducing CoT token counts by over 45% on average and delivering  $1.6\times$ - $2.0\times$  inference speedups—while maintaining high reasoning accuracy. Notably, it significantly outperforms existing baselines by preserving accuracy even at high effective compression rates, advancing the state of the art in the CoT reasoning efficiency-accuracy trade-off.

## 1 Introduction

Large Language Models (LLMs) excel at complex reasoning, significantly advanced by Chain-of-Thought (CoT) prompting [47] which enables step-by-step deliberation, enhancing performance and interpretability. Specialized Large Reasoning Models (LRMs) like DeepSeek-R1 [13] and OpenAI’s o1 [17] further advance reasoning, often generating extremely long, structured CoT sequences [28, 40]. However, this increased reasoning depth leads to verbose CoT sequences whose autoregressive generation [44] incurs substantial computational costs, latency, and memory demands—a major practical bottleneck. While researchers actively pursue general LLM efficiency improvements [34, 21, 39, 45], optimizing CoT reasoning efficiency itself remains a critical, distinct challenge.

Beyond sequence length, LLM-generated CoT traces are often qualitatively inefficient [28]. Studies reveal common redundancies: repetitive phrasing, unnecessary verifications, and over-analysis of simple sub-problems [10]. This overthinking [40] wastes resources and can degrade reasoning by introducing noise or errors, especially with long traces for simple tasks [50]. Thus, enabling models to achieve a thinking-optimal state, in other words reasoning just enough by dynamically tailoring

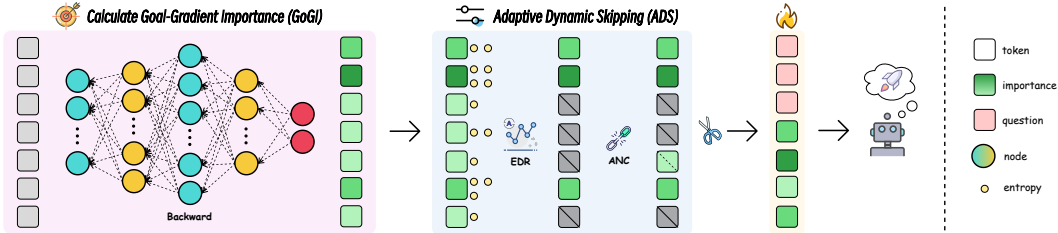


Figure 1: **Building an accelerated language model with Adaptive GoGI-Skip framework.** (a) Calculating GoGI by measuring the gradient influence of each token’s intermediate representation on the final answer loss for an original CoT. (b) Applying ADS, informed by EDR regulation and ANC, to determine which tokens to prune based on both importance and local context. (c) This dynamically compressed CoT data then fine-tunes a base LLM, enabling efficient inference without requiring additional parameters at runtime.

reasoning depth and verbosity to the problem—optimizing for true reasoning efficiency, or Redundant In, Compressed Out (RICO)—is critical.

Existing CoT compression approaches, particularly Supervised Fine-Tuning (SFT) methods like token skipping [48], show promise but face fundamental limitations. They often use generic importance metrics like semantic similarity [26] or perplexity-based local predictability [7] which misaligned with the actual reasoning goal. Consequently, they may fail to preserve functionally critical tokens, especially those semantically simple yet structurally vital [29]. An effective metric must be goal-oriented, assessing a token’s functional contribution to the correct answer. Secondly, static compression rates, common in token skipping, ignore reasoning’s dynamic nature, where phases demand varying scrutiny. While adaptive computation paradigms exist [34], integrating runtime adaptivity with SFT-learned token-level CoT compression remains largely unexplored.

To bridge these gaps, we propose Adaptive GoGI-Skip, a framework for learning efficient, adaptive CoT compression. Our approach, as illustrated in Figure 1, integrates two synergistic innovations: Goal-Gradient Importance (GoGI), a novel metric ( $\mathcal{G}(x_i, l) = \|\nabla_{h_t^l} \mathcal{L}_{\text{ans}}\|_1$ ) quantifying a token  $x_i$ ’s functional importance at layer  $l$  via its influence on the final answer loss  $\mathcal{L}_{\text{ans}}$  and Adaptive Dynamic Skipping (ADS). ADS uses Entropy-Driven Rate (EDR) Regulation (leveraging predictive entropy  $H_t$  to adjust retention  $\gamma_t$ ) and an Adaptive N-Constraint (ANC) (modulating consecutive deletions based on local contextual complexity) to ensure coherence.

Our key contributions include:

- The first CoT compression framework unifying goal-oriented, gradient-based importance with dynamic, uncertainty-aware skipping via SFT.
- GoGI, a principled importance metric, and ADS (with EDR and ANC), a novel dynamic mechanism, for targeted, adaptive, robust compression.
- A demonstration of state-of-the-art efficiency and accuracy on diverse benchmarks with >45% token reduction and 1.6-2.0× speedup, preserving accuracy.

## 2 Related Work

Improving reasoning efficiency, particularly via fine-tuning, is an active research area [28, 40]. Existing SFT-based CoT compression techniques differ mainly in token importance assessment and compression strategies.

**Token Importance** Some methods employ external compressors, such as GPT-4 for distillation [19]. Others utilize LLM-internal signals, including semantic relevance from tools like LLMLingua [26] (used by TokenSkip [48]), or token predictability measured by perplexity changes, as in SPIRIT [7]. These generic metrics often misalign with the reasoning goal, potentially discarding functionally critical tokens [29]. In contrast, our GoGI directly measures a token’s influence on the final answer loss, providing a truly goal-oriented signal.

**Compression Strategy** Existing SFT-based methods often employ static rates, as seen in TokenSkip [48], or coarse step-skipping [22], failing to adapt to varying reasoning complexity or risking coherence loss. Our ADS overcomes this via fine-grained, runtime adaptivity. Its EDR regulation and ANC dynamically adjust compression based on model uncertainty and local context, balancing efficiency and coherence more optimally.

**Other Paradigms** While various paradigms offer promising avenues for enhancing CoT efficiency, they typically prioritize different aspects of the solution space compared to our SFT-based token skipping framework. Latent-space reasoning [33, 14, 3] reasons in hidden states, sacrificing CoT interpretability and performance [24]. Reinforcement Learning (RL) approaches [23, 35, 52] optimize rewards with length penalties, facing complex reward shaping and training instability. Inference-time methods [25, 51, 45] alter decoding without fine-tuning model parameters. Our SFT-based token skipping offers a distinct balance.

### 3 Adaptive GoGI-Skip for achieving RICO

To address limitations of static/generic CoT compression, we propose Adaptive GoGI-Skip (Figure 1), an SFT framework for learning dynamic pruning aiming for RICO. It synergistically integrates: (1) Goal-Gradient Importance (GoGI) to quantify a token’s functional contribution to the answer loss; and (2) Adaptive Dynamic Skipping (ADS), which uses Entropy-Driven Rate (EDR) regulation for uncertainty-based pruning intensity and an Adaptive N-Constraint (ANC) for local coherence. This combination of goal-oriented importance and dynamic context-aware adaptation yields more nuanced, effective compression than prior methods. GoGI and ADS are detailed below.

**Notation.** Sequences are denoted as  $(x_t)_{t=1}^m$ . Vectors are bold lowercase (e.g.,  $\mathbf{h}_t^l$  for hidden state of token  $t$  at layer  $l$ ). Key metrics include GoGI score  $\mathcal{G}_t$ , predictive entropy  $H_t$ , dynamic retention rate  $\gamma_t$ , dynamic GoGI threshold  $\tau_t$ , and adaptive N-constraint  $N_t$ .  $K_t \in \{0, 1\}$  is the keep decision indicator.  $\mathcal{L}_{\text{ans}}$  denotes the answer loss. Model parameters are  $\theta$ . We use standard mathematical operators:  $\|\cdot\|_1$  (L1 norm),  $\nabla$  (gradient),  $Q_p(\cdot)$  (the  $p$ -th percentile),  $[\cdot]_{\text{low}}^{\text{high}}$  (clipping to the range [low, high]),  $\lfloor \cdot \rfloor$  (floor),  $\mathbb{I}(\cdot)$  (indicator function),  $\vee$  (logical OR), and  $\wedge$  (logical AND). Appendix A details hyperparameters such as  $\gamma_{\min}$  and  $N_{\max}$ .

#### 3.1 Goal-Gradient Importance (GoGI)

Existing importance metrics [48, 26, 7, 29] lack a direct connection to the reasoning objective. To address this, we introduce the GoGI score to directly quantify a token’s functional contribution towards deriving the final correct answer.

Given a CoT sequence  $c = (x_t)_{t=1}^m$  and answer  $A = (a_t)_{t=1}^k$ , the answer prediction loss  $\mathcal{L}_{\text{ans}}$  for model  $M_\theta$  is:

$$\mathcal{L}_{\text{ans}}(A|c; \theta) = - \sum_{j=1}^k \log P_\theta(a_j | c, a_{<j}) \quad (1)$$

The GoGI score for token  $x_t$  at target layer  $l^*$  is the L1 norm of the gradient:

$$\mathcal{G}_t^{(l^*)} \triangleq \left\| \frac{\partial \mathcal{L}_{\text{ans}}(A|c; \theta)}{\partial \mathbf{h}_t^{l^*}} \right\|_1 \quad (2)$$

This score measures the local sensitivity of the final answer loss to the intermediate representation  $\mathbf{h}_t^{l^*}$ .

The choice of the target layer  $l^*$  influences the characteristics of the captured importance signals, necessitating a principled selection process. To determine an appropriate  $l^*$ , our analysis (further detailed in Appendix A) considers layer-wise gradient contributions to next-token prediction logits as a proxy for layer activity, alongside full GoGI score statistics computed for a subset of layers. We observe peak sensitivity and importance concentration in the latter middle-to-late layers. Specifically, for the 34-layer Gemma3-4B-Instruct model, while high maximum GoGI values appear at both Layer 23 and Layer 28, Layer 23 exhibits a stronger overall contribution signal (reflected in its median and variance in the boxplot). Therefore, balancing peak sensitivity with overall contribution, we select Layer 23 as the default target layer  $l^*$ . We then denote  $\mathcal{G}_t = \mathcal{G}_t^{(l^*)}$ . Optional token type-weighting,

$\mathcal{G}_{w,t} = w_t \cdot \mathcal{G}_t$  (where weights  $w_t$  are detailed in Appendix A), can be applied. The score used for pruning, denoted  $\mathcal{G}'_t$ , is  $\mathcal{G}_{w,t}$  if type-weighting is enabled, and  $\mathcal{G}_t$  otherwise.

### 3.2 Adaptive Dynamic Skipping (ADS)

ADS dynamically adjusts the pruning strategy based on runtime context, primarily through its EDR and ANC components.

#### 3.2.1 Entropy-Driven Rate (EDR) Regulation

To adapt compression intensity, EDR regulation uses predictive entropy  $H_t$  (Eq. 3) as an uncertainty signal. High entropy implies complexity, warranting conservative pruning (i.e.,  $\gamma_t \uparrow$ ), while low entropy allows aggressive pruning (i.e.,  $\gamma_t \downarrow$ ). As detailed in Appendix D,  $H_t$  and  $\mathcal{G}_t$  are largely uncorrelated, thereby providing complementary information for pruning decisions.

$$H_t = - \sum_{v \in \mathcal{V}} p_{t,v} \log p_{t,v}, \quad (3)$$

where  $p_{t,v} = P_\theta(X_{t+1} = v | x_1, \dots, x_t)$  and  $\mathcal{V}$  is the vocabulary set. To leverage this complementarity, we first map  $H_t$  to a normalized value  $\hat{H}_t \in [0, 1]$  using a mapping function  $\mathcal{M}(\cdot; \theta_{\mathcal{M}})$  (details in Appendix A):

$$\hat{H}_t = \mathcal{M}(H_t; \theta_{\mathcal{M}}) \quad (4)$$

Based on  $\hat{H}_t$ , the local retention rate  $\gamma_t$  is calculated as:

$$\gamma_t = [\gamma_{\min} + (\gamma_{\max} - \gamma_{\min}) \cdot \hat{H}_t]_{\gamma_{\min}^{\text{abs\_max}}}^{\gamma_{\max}^{\text{abs\_min}}} \quad (5)$$

where  $\gamma_{\min}$  and  $\gamma_{\max}$  are base retention rate bounds, and the outer notation  $[\cdot]_{\gamma_{\min}^{\text{abs\_min}}}^{\gamma_{\max}^{\text{abs\_max}}}$  indicates that the resulting value is clipped to the absolute range  $[\gamma_{\min}^{\text{abs\_min}}, \gamma_{\max}^{\text{abs\_max}}]$  (hyperparameters detailed in Appendix A). This retention rate then informs the dynamic GoGI threshold  $\tau_t$ , which is the  $(1 - \gamma_t) \times 100$ -th percentile of relevant GoGI scores (denoted  $Q_{(1-\gamma_t) \times 100}(\cdot)$ ):

$$\tau_t = Q_{(1-\gamma_t) \times 100}(\{\mathcal{G}_j | j \in \mathcal{I}_{\text{valid}}\}) \quad (6)$$

where  $\mathcal{I}_{\text{valid}}$  excludes non-substantive tokens (e.g., padding, special formatting tokens, as detailed in Appendix A).

#### 3.2.2 Adaptive N-Constraint (ANC) for Coherence

To prevent disrupting cognitive coherence, the ANC dynamically limits the number of consecutive pruned ( $N_t$ ) based on local complexity. This complexity is estimated via a windowed average of predictive entropy,  $\bar{H}_{t,W}$  (Eq. 7). After normalizing  $\bar{H}_{t,W}$  to  $\hat{\bar{H}}_{t,W}$  using a mapping function  $\mathcal{M}'$  (details in Appendix A), the adaptive constraint  $N_t$  is computed as (Eq. 9):

$$\bar{H}_{t,W} = \frac{1}{W} \sum_{j=[t-W//2]_1}^{[t+W//2]_m} H_j \quad (7)$$

$$\hat{\bar{H}}_{t,W} = \mathcal{M}'(\bar{H}_{t,W}; \theta_{\mathcal{M}'}) \quad (8)$$

$$N_t = \left\lfloor \text{clip} \left( N_{\min} + (N_{\max} - N_{\min}) \cdot (1 - \hat{\bar{H}}_{t,W}), N_{\min}, N_{\max} \right) + 0.5 \right\rfloor \quad (9)$$

Consequently, high local entropy (a high  $\hat{\bar{H}}_{t,W}$ ) leads to a smaller  $N_t$  (more conservative pruning), while low local entropy allows for a larger  $N_t$ .

### 3.3 Adaptive GoGI-Skip Pruning Algorithm

The final pruning decision for each token  $x_t$  integrates its GoGI score with the EDR and ANC mechanisms. Let  $C_{t-1}$  be the count of consecutively pruned tokens preceding  $x_t$  ( $C_0 = 0$ ). The keep decision indicator  $K_t \in \{0, 1\}$  for  $x_t$  is then determined by Eq. 10:

$$K_t = \mathbb{I}(\mathcal{G}'_t \geq \tau_t) \vee (\mathbb{I}(\mathcal{G}'_t < \tau_t) \wedge \mathbb{I}(C_{t-1} + 1 \geq N_t)) \quad (10)$$

The consecutive prune counter  $C_t$  is updated as  $C_t = (C_{t-1} + 1)(1 - K_t)$ . This entire algorithm is applied offline to the original CoT sequences to generate the compressed versions  $c'_{\text{comp}} = (x_t)_{K_t=1}$  used for subsequent fine-tuning.

## 4 Experiments

This section evaluates Adaptive GoGI-Skip through experiments. We describe the experimental setup, then showing its effectiveness in efficiency and accuracy across benchmarks and model variants in main results, and analyze core component contributions via ablation studies.

### 4.1 Experimental Setup

**Models** Our experiments employ two families of state-of-the-art open-source instruction-tuned models: Google’s Gemma3-Instruct series (1B/4B/12B) [42] and Qwen2.5-Instruct series (3B/7B) [49]. This diverse selection facilitates a thorough evaluation of our approach’s scalability with model size and its generalizability across different architectural designs.

**Training Data** We began by sourcing 7,500 samples from the MATH training dataset [15], which contains mathematical problems and their reference CoT solutions. After format standardization and parsing validation (detailed in Appendix A), 7,472 valid samples were obtained. The core training dataset for Adaptive GoGI-Skip was then generated by applying our pruning algorithm to these validated samples. Correspondingly, for all baseline methods, their respective training datasets were generated by applying their specific techniques to the same set of 7,472 validated source CoT solutions.

**Baselines** We evaluated Adaptive GoGI-Skip against several baselines: (1) *Original*: standard CoT generation without any compression; (2) *Prompting*: zero-shot prompting intended to elicit concise reasoning (details in Appendix B); (3) *C3ot*: CoT compression using an external model as the compressor [19]; (4) *Spiritft*: pruning based on stepwise perplexity changes [7]; and (5) *TokenSkip*: token-level skipping with pre-defined target retention ratios ( $\gamma$ ) of 0.5 and 0.6 [48].

**Implementation Details** We computed GoGI scores at an optimal target layer, determined per model family via gradient contribution analysis. Key hyperparameters for the ADS mechanism, such as retention rate bounds and consecutive skip constraints, were fixed across experiments. All SFT-based methods, including ours, were fine-tuned using Low-Rank Adaptation (LoRA) [16] on 3 NVIDIA 4090 GPUs. All evaluations employed greedy decoding. Comprehensive details regarding GoGI layer selection, specific ADS parameters, LoRA configurations, and other SFT settings are provided in Appendix A.

### 4.2 Main Results

Our experiments demonstrate that Adaptive GoGI-Skip significantly enhances CoT reasoning efficiency across various models and benchmarks while robustly preserving accuracy, generally outperforming existing static compression techniques. To ensure result stability, all accuracy metrics reported in this section represent averages from 3 independent fine-tuning runs, each employing a different random seed.

The results for Gemma3-4B-it, detailed in Table 1, show that Adaptive GoGI-Skip consistently achieves a demonstrably superior efficiency-accuracy balance relative to all baselines. It delivers remarkable speedups over the Original CoT, ranging from approximately  $1.7\times$  on challenging AIME benchmarks to  $2.2\times$  on GSM8K. This efficiency stems from its dynamic adjustment of the token retention ratio. For instance, on complex tasks like AIME benchmarks, this ratio averages approximately 0.6, while for simpler tasks such as GSM8K, it decreases to around 0.45. Crucially, Adaptive GoGI-Skip achieves these efficiency gains with minimal impact on accuracy, exhibiting negligible drops of 0.3-0.4% on GPQA Diamond and AIME’24, and even a slight 0.3% improvement on GSM8K. Even its largest accuracy decrease, 0.9% on the challenging AIME’25 benchmark,

<sup>1</sup><https://huggingface.co/datasets/math-ai/aime25>

<sup>2</sup><https://huggingface.co/datasets/math-ai/aime24>

Table 1: **Performance comparison of different strategies on Gemma3-4B-it across various reasoning benchmarks.** Ratio indicates the average proportion of tokens retained compared to the Original CoT length. Speedup measures the reduction in end-to-end inference latency relative to the Original CoT.  $\gamma$  denotes the target retention ratio for the TokenSkip baseline. Subscripted values next to accuracy scores indicate the absolute percentage point change compared to the Original.

Method	AIME 2025 <sup>1</sup>				AIME 2024 <sup>2</sup>			
	Acc.↑	Ratio↓	Tokens↓	Speedup↑	Acc.↑	Ratio↓	Tokens↓	Speedup↑
Original	6.1 <sub>(0.01)</sub>	1.0	832	1.0×	14.5 <sub>(0.01)</sub>	1.0	804	1.0×
Prompting	1.8 <sub>(4.31)</sub>	0.9	764	1.0×	10.2 <sub>(4.31)</sub>	0.9	728	1.1×
C3ot	2.6 <sub>(3.54)</sub>	0.7	564	1.4×	13.1 <sub>(1.41)</sub>	0.7	552	1.4×
Spiritft	3.6 <sub>(2.54)</sub>	0.6	556	1.5×	13.7 <sub>(0.84)</sub>	0.7	544	1.4×
TokenSkip ( $\gamma = 0.6$ )	4.1 <sub>(2.01)</sub>	0.6	523	1.6×	12.6 <sub>(1.91)</sub>	0.6	512	1.5×
TokenSkip ( $\gamma = 0.5$ )	2.7 <sub>(3.41)</sub>	0.6	457	1.7×	11.3 <sub>(3.21)</sub>	0.5	448	1.6×
Adaptive GoGI-Skip (Ours)	5.2 <sub>(0.91)</sub>	0.6	481	1.6×	14.1 <sub>(0.41)</sub>	0.6	456	1.7×

Method	GPQA Diamond [30]				GSM8K [5]			
	Acc.↑	Ratio↓	Tokens↓	Speedup↑	Acc.↑	Ratio↓	Tokens↓	Speedup↑
Original	29.6 <sub>(0.04)</sub>	1.0	713	1.0×	89.6 <sub>(0.04)</sub>	1.0	258	1.0×
Prompting	21.7 <sub>(7.94)</sub>	0.9	651	1.0×	80.2 <sub>(9.41)</sub>	0.9	225	1.1×
C3ot	28.4 <sub>(1.24)</sub>	0.7	469	1.5×	89.5 <sub>(0.14)</sub>	0.6	165	1.5×
Spiritft	28.1 <sub>(1.54)</sub>	0.6	462	1.5×	89.2 <sub>(0.41)</sub>	0.6	163	1.5×
TokenSkip ( $\gamma = 0.6$ )	28.0 <sub>(1.64)</sub>	0.6	434	1.6×	88.4 <sub>(1.21)</sub>	0.6	153	1.6×
TokenSkip ( $\gamma = 0.5$ )	26.5 <sub>(3.11)</sub>	0.5	378	1.8×	84.3 <sub>(5.01)</sub>	0.5	133	1.9×
Adaptive GoGI-Skip (Ours)	29.3 <sub>(0.34)</sub>	0.5	371	1.8×	89.9 <sub>(0.31)</sub>	0.4	113	1.9×

results in a score that remains highly competitive. In contrast, static baselines exhibit a rigid trade-off: aggressive compression (e.g., TokenSkip with  $\gamma = 0.5$ ) yields high speedups (around  $1.8\times$ ) but incurs significant accuracy drops (3-5%), whereas conservative static methods offer lower speedups (around  $1.4\times$ - $1.6\times$ ) to better preserve accuracy. Adaptive GoGI-Skip surpasses this static compromise: it dynamically adapts to robustly match the original model’s accuracy while achieving efficiency levels comparable to those of aggressive static pruning techniques. The performance of the Prompting baseline further underscores that fine-tuning is essential for achieving effective CoT compression.

Table 2: **Generalization performance across different model sizes and architectures.** The best and second best results are highlighted in **bold** and underlined, respectively. SU. denotes Speedup.

Method	Gemma3-1B-It								Gemma3-12B-It							
	AIME'25		AIME'24		GPQA		GSM8K		AIME'25		AIME'24		GPQA		GSM8K	
	Acc.	SU.	Acc.	SU.	Acc.	SU.	Acc.	SU.	Acc.	SU.	Acc.	SU.	Acc.	SU.	Acc.	SU.
Original	<b>0.7</b>	1.0×	<b>3.1</b>	1.0×	<b>18.7</b>	1.0×	<b>70.2</b>	1.0×	<b>8.1</b>	1.0×	<u>22.7</u>	1.0×	<b>38.4</b>	1.0×	<u>95.2</u>	1.0×
Prompting	0.1	1.1×	1.2	1.1×	12.5	1.1×	65.7	1.1×	4.2	1.1×	15.3	1.1×	28.7	1.1×	85.6	1.1×
C3ot	0.5	1.4×	2.3	1.4×	16.1	1.4×	68.7	1.5×	7.4	1.4×	21.6	1.5×	<u>37.4</u>	1.5×	94.1	1.5×
Spiritft	0.4	1.4×	2.1	1.4×	17.3	1.5×	69.6	1.5×	7.2	1.5×	21.2	1.5×	36.6	1.5×	93.8	1.6×
TokenSkip ( $\gamma=0.6$ )	0.5	1.5×	2.2	1.5×	16.5	1.5×	69.9	1.6×	7.5	1.5×	21.9	1.6×	37.1	1.6×	94.3	1.6×
TokenSkip ( $\gamma=0.5$ )	0.3	1.6×	1.9	1.6×	15.8	1.6×	64.6	1.7×	6.8	1.6×	21.2	1.8×	36.1	1.7×	92.7	1.8×
Adaptive GoGI-Skip	<u>0.6</u>	1.5×	<u>2.9</u>	1.5×	<u>18.4</u>	1.6×	<b>70.2</b>	1.8×	<u>8.0</u>	1.6×	<b>22.9</b>	1.7×	<b>38.4</b>	1.7×	<b>95.5</b>	2.0×

Method	Qwen2.5-3B-It								Qwen2.5-7B-It							
	AIME'25		AIME'24		GPQA		GSM8K		AIME'25		AIME'24		GPQA		GSM8K	
	Acc.	SU.	Acc.	SU.	Acc.	SU.	Acc.	SU.	Acc.	SU.	Acc.	SU.	Acc.	SU.	Acc.	SU.
Original	<b>2.1</b>	1.0×	<b>7.5</b>	1.0×	<b>25.3</b>	1.0×	<u>78.5</u>	1.0×	<b>6.2</b>	1.0×	<b>18.1</b>	1.0×	<b>35.7</b>	1.0×	<u>84.5</u>	1.0×
Prompting	0.8	1.1×	4.1	1.1×	17.2	1.1×	65.3	1.1×	2.8	1.1×	11.2	1.1×	25.8	1.1×	77.1	1.1×
C3ot	1.7	1.4×	6.8	1.4×	23.5	1.5×	76.1	1.5×	5.6	1.5×	17.0	1.5×	<u>34.3</u>	1.5×	82.7	1.5×
Spiritft	1.6	1.5×	6.5	1.5×	23.0	1.5×	75.2	1.5×	5.3	1.5×	16.6	1.5×	33.6	1.5×	88.2	1.6×
TokenSkip ( $\gamma=0.6$ )	1.8	1.5×	6.9	1.6×	23.4	1.6×	76.5	1.6×	5.7	1.6×	<u>17.2</u>	1.6×	34.1	1.6×	83.1	1.6×
TokenSkip ( $\gamma=0.5$ )	1.4	1.6×	5.8	1.6×	22.5	1.7×	73.8	1.9×	5.4	1.7×	15.8	1.7×	32.9	1.7×	81.5	1.9×
Adaptive GoGI-Skip	<u>2.0</u>	1.5×	<u>7.3</u>	1.5×	<u>24.6</u>	1.7×	<b>78.9</b>	1.8×	<u>6.1</u>	1.5×	<b>18.1</b>	1.5×	<b>35.7</b>	1.6×	<b>85.1</b>	1.9×

The generalization capabilities of Adaptive GoGI-Skip are demonstrated by further experiments detailed in Table 2, which confirm its robustness and scalability across these diverse models. Whether applied to smaller models like Gemma3-1B-it and Qwen2.5-3B-it or larger ones like Gemma3-12B-it and Qwen2.5-7B-it, our method consistently maintains accuracy closely aligned with that of the corresponding original models. Simultaneously, Adaptive GoGI-Skip delivers significant, task-adaptive speedups, which typically range from  $1.8\times$  to  $2.0\times$  on GSM8K across different model scales. This favorable performance profile, particularly on smaller models where static pruning

typically incurs larger accuracy penalties, contrasts with that of the representative static baseline TokenSkip. These consistent results strongly suggest that Adaptive GoGI-Skip offers a broadly applicable strategy for efficient CoT reasoning.

### 4.3 Analysis

**The Effectiveness of Adaptive GoGI-Skip** To understand the effectiveness of Adaptive GoGI-Skip, we first delve into the properties of its core components. The GoGI score, as illustrated by its distribution in Figure 2 (left), is highly skewed: a small fraction of tokens accounts for the majority of functional importance within CoT sequences, providing a strong theoretical basis for selective pruning. Crucially, this GoGI metric captures a unique dimension of importance that, being largely uncorrelated with runtime predictive entropy (correlation analysis in Appendix D), offers complementary signals for pruning decisions.

**Dynamic Behavior of ADS** The ADS mechanism effectively leverages the characteristics of GoGI scores. For instance, Figure 2 (right) visualizes how its EDR determined local token retention rate ( $\gamma_t$ ) dynamically responds to multiple factors, including runtime uncertainty and intrinsic problem characteristics proxied by original CoT length and overall GoGI levels. This visualization confirms that EDR regulation adaptively adjusts compression intensity based on the immediate context. Furthermore, its ANC component ensures local coherence. Appendix F illustrates an instance where ANC preserves a structurally important token with a low GoGI score by dynamically limiting consecutive skips based on local entropy statistics, thereby maintaining logical flow.

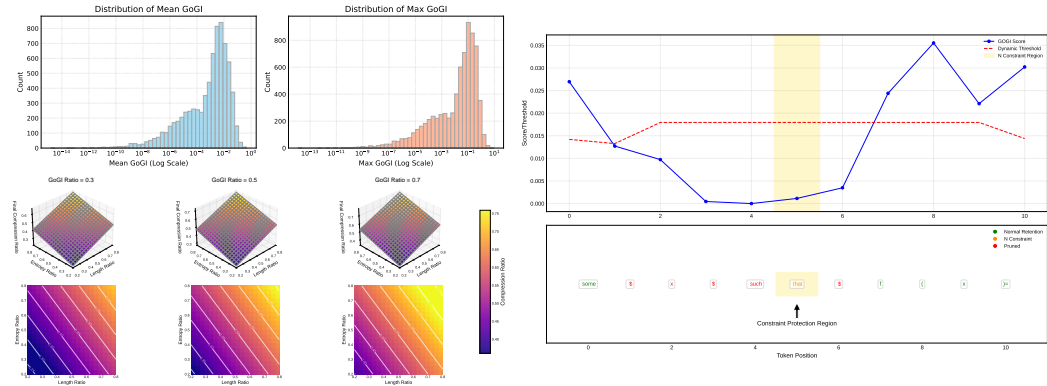


Figure 2: **GoGI score characteristics and dynamic behavior of Adaptive GoGI-Skip.** **Left:** The highly skewed distribution of GoGI scores from 7,472 MATH training samples. **Right:** Illustration of the dynamic token retention rate’s multi-faceted response to runtime entropy, original CoT length, and overall GoGI score distribution. The color gradient indicates the average GoGI score of the tokens retained by the dynamic mechanism.

**Ablation Study** To quantify the distinct and synergistic contributions of its core components, we conducted an ablation study (results in Table 3). The findings are as follows: Removing ANC while retaining GoGI and EDR (the GoGI+EDR variant) causes a noticeable drop in accuracy, particularly on challenging AIME benchmarks, despite slightly higher speedups on simpler tasks like GSM8K. This result underscores ANC’s crucial role in preserving coherence and preventing critical information loss, even if it slightly tempers maximum compression. Disabling EDR regulation and employing a static retention ratio (GoGI+ANC Static Rate variant) alongside GoGI and ANC yields a marked decrease in average speedup across most tasks compared to the full method, highlighting EDR’s effectiveness in dynamically adapting compression for superior overall efficiency. Notably, removing the entire ADS mechanism (the ‘w/o ADS’ variant) results in the most substantial accuracy degradation across benchmarks, emphasizing the critical combined contribution of EDR and ANC. Moreover, replacing GoGI with a generic importance metric (the LLMInguua+ADS variant) while retaining the dynamic ADS mechanism leads to consistently lower accuracy across all benchmarks. This demonstrates the significant advantage of our goal-oriented GoGI scores in identifying functionally critical tokens. Consequently, the full Adaptive GoGI-Skip framework, synergizing GoGI with both EDR and ANC,

Table 3: **Ablation study results on Gemma-3-4B-it, isolating contributions of GoGI and ADS.** The notation w/o indicates the removal of the specified component. The term GoGI-Static in method variant names denotes implementations that use GoGI for importance but with a fixed retention ratio ( $\gamma$ ) instead of dynamic EDR. The LLMLingua+ADS variant replaces GoGI scores with LLMLingua-derived importance scores while retaining the dynamic EDR and ANC mechanisms.

Method Variant	AIME 2025		AIME 2024		GPQA Diamond		GSM8K	
	Acc.	Speedup	Acc.	Speedup	Acc.	Speedup	Acc.	Speedup
Full Method (GoGI+EDR+ANC)	5.2	1.6×	14.1	1.7×	29.3	1.8×	89.9	1.9×
w/o ANC (GoGI+EDR only)	4.5 <sub>(0.7↓)</sub>	1.7×	13.6 <sub>(0.5↓)</sub>	1.8×	28.5 <sub>(0.8↓)</sub>	1.9×	89.0 <sub>(0.9↓)</sub>	2.0×
w/o EDR (GoGI-Static, $\gamma \approx 0.5$ )	4.3 <sub>(0.9↓)</sub>	1.6×	13.5 <sub>(0.6↓)</sub>	1.5×	28.6 <sub>(0.7↓)</sub>	1.6×	89.5 <sub>(0.4↓)</sub>	1.6×
w/o ADS (GoGI-Static, $\gamma \approx 0.5$ )	4.0 <sub>(1.2↓)</sub>	1.9×	13.0 <sub>(1.1↓)</sub>	1.9×	28.0 <sub>(1.3↓)</sub>	1.9×	88.5 <sub>(1.4↓)</sub>	1.9×
w/o GoGI (LLMLingua+ADS)	4.6 <sub>(0.6↓)</sub>	1.6×	13.8 <sub>(0.3↓)</sub>	1.7×	28.8 <sub>(0.5↓)</sub>	1.8×	89.1 <sub>(0.8↓)</sub>	1.9×

thus consistently achieves an optimal balance of high accuracy and efficiency, confirming that each of its core components makes a substantial and complementary contribution.

## 5 Discussion

Our experiments demonstrate the effectiveness of Adaptive GoGI-Skip in enhancing CoT reasoning efficiency while robustly preserving accuracy. This section elaborates on key insights from our method and findings. We contextualize these within the broader scientific landscape, acknowledge current limitations, and outline promising future research directions.

### 5.1 Targeting Functional Relevance Beyond Surface Statistics

The proposed GoGI score is pivotal because it directly links token importance to the final reasoning objective, thereby offering a distinct advantage over generic metrics [48, 26, 7]. It quantifies functional relevance using answer loss gradients. Our analysis demonstrates that GoGI scores exhibit high sparsity, indicating that functional importance within CoT sequences is primarily concentrated in a relatively small subset of tokens. Figure 3 (left) visually underscores this near-orthogonality, revealing no strong linear correlation between per-token GoGI scores and predictive entropy values. This lack of correlation—further confirmed by our quantitative correlation analysis (detailed in Appendix D)—highlights that GoGI captures a distinct, goal-oriented dimension of importance, which is complementary to runtime uncertainty signals such as entropy. This underscores the necessity of goal-oriented metrics. From a broader perspective, GoGI’s focus on gradient-based influence resonates with interpretability research [9, 46, 41, 37], its goal-directed contribution aligns conceptually with causal inference frameworks [27, 32, 31], and its function-over-form approach resonates with findings on simple token importance [29] and perhaps finds an echo in neuroscientific functional specialization [2, 1].

### 5.2 Adaptive Skipping for Coherent Efficiency

The ADS mechanism effectively balances efficiency and coherence, and draws compelling parallels with adaptive cognitive processes, such as those described in dual-process theories [18, 36, 8]. Its EDR component dynamically adjusts compression intensity based on runtime uncertainty: high entropy leads to conservative pruning, akin to deliberate System 2 reasoning [38], while low entropy permits aggressive skipping mirroring intuitive System 1 processing [43, 20]. This allows dynamic allocation of the computational budget—thinking slowly only when necessary. Complementing EDR, the ANC component further ensures coherence by dynamically limiting consecutive skips based on local context stability, as Figure 3 (right) illustrates. This prevents disruption of cognitive coherence and implicitly protects structurally important tokens—even those with low GoGI scores—by adapting the pruning constraint ( $N_t$ ) based on local informational flux as proxied by entropy stability [12, 11, 4]. This synergy between rate adaptation and coherence protection allows Adaptive GoGI-Skip to intrinsically navigate the efficiency-accuracy trade-off by dynamically approximating task-optimal reasoning lengths and thereby mitigating the overthinking phenomenon.

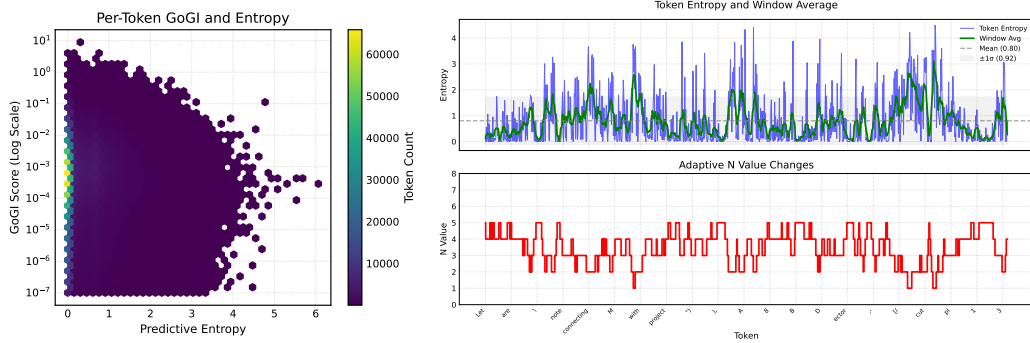


Figure 3: **Properties of GoGI and the ANC Mechanism.** **Left:** A hexbin plot of per-token GoGI scores versus predictive entropy illustrates their near-orthogonality, suggesting GoGI captures a distinct dimension of importance. **Right:** The ANC mechanism dynamically adjusts the maximum number of consecutive token skips ( $N_t$ ) based on local contextual stability (derived from windowed predictive entropy), thereby ensuring reasoning coherence.

### 5.3 Limitation and Future Work

Despite Adaptive GoGI-Skip shows strong performance, its full potential warrants further investigation in two key directions. Given that the core principles of goal-gradient importance and dynamic skipping are model-and-task agnostic, we expect robust generalization to a wider array of LLM architectures and substantially broader reasoning domains. Furthermore, the experiments in this work validated Adaptive GoGI-Skip by compressing pre-existing CoT data. We anticipate that applying our methodology directly to compress a model’s own natively generated reasoning trajectories could yield even more natural and efficient compressed thought processes, potentially leading to further performance gains.

Beyond such empirical validation, a highly promising future direction involves pursuing end-to-end learned efficiency using RL. We are actively exploring RL frameworks to train models that autonomously learn optimal skipping or resource allocation policies. Key research questions in this RL domain include the meticulous design of composite reward functions—balancing task success against multi-faceted efficiency costs—and the significant challenge of ensuring stable and scalable large-scale RL training protocols. Successfully addressing these could enable models to intrinsically manage their reasoning processes for true thinking-optimal performance.

## 6 Conclusion

We introduced Adaptive GoGI-Skip, a novel framework to address CoT inefficiency in LLMs. This framework uniquely integrates the GoGI metric with the ADS mechanism. Learned via supervised fine-tuning, Adaptive GoGI-Skip demonstrates a superior efficiency-accuracy trade-off across diverse models and benchmarks, achieving substantial average token reductions exceeding 45% which translate to task-dependent inference speedups between  $1.6\times$  and  $2.0\times$ . Crucially, unlike static compression techniques that typically sacrifice accuracy for efficiency, our method robustly preserves reasoning accuracy even at these high average efficiency levels. Consequently, it significantly outperforms existing baselines and establishes a new state-of-the-art in efficient, high-fidelity CoT reasoning. This work underscores the significant potential of combining goal-oriented importance metrics with dynamic adaptation strategies, paving the way towards more practical and thinking-optimal LLMs.

## References

- [1] Danielle S Bassett and Olaf Sporns. Network neuroscience. *Nature neuroscience*, 20(3):353–364, 2017.
- [2] Steven L Bressler and Vinod Menon. Large-scale brain networks in cognition: emerging methods and principles. *Trends in cognitive sciences*, 14(6):277–290, 2010.

- [3] Jeffrey Cheng and Benjamin Van Durme. Compressed chain of thought: Efficient reasoning through dense representations. *arXiv preprint arXiv:2412.13171*, 2024.
- [4] Kevin Clark, Urvashi Khandelwal, Omer Levy, and Christopher D Manning. What does bert look at? an analysis of bert’s attention. *arXiv preprint arXiv:1906.04341*, 2019.
- [5] Karl Cobbe, Vineet Kosaraju, Mohammad Bavarian, Mark Chen, Heewoo Jun, Lukasz Kaiser, Matthias Plappert, Jerry Tworek, Jacob Hilton, Reiichiro Nakano, Christopher Hesse, and John Schulman. Training verifiers to solve math word problems. *arXiv preprint arXiv:2110.14168*, 2021.
- [6] Alexis Conneau, Kartikay Khandelwal, Naman Goyal, Vishrav Chaudhary, Guillaume Wenzek, Francisco Guzmán, Edouard Grave, Myle Ott, Luke Zettlemoyer, and Veselin Stoyanov. Unsupervised cross-lingual representation learning at scale. *arXiv preprint arXiv:1911.02116*, 2019.
- [7] Yingqian Cui, Pengfei He, Jingying Zeng, Hui Liu, Xianfeng Tang, Zhenwei Dai, Yan Han, Chen Luo, Jing Huang, Zhen Li, et al. Stepwise perplexity-guided refinement for efficient chain-of-thought reasoning in large language models. *arXiv preprint arXiv:2502.13260*, 2025.
- [8] Nathaniel D Daw, Yael Niv, and Peter Dayan. Uncertainty-based competition between prefrontal and dorsolateral striatal systems for behavioral control. *Nature neuroscience*, 8(12):1704–1711, 2005.
- [9] Kevin Du, Lucas Torroba Hennigen, Niklas Stoehr, Alexander Warstadt, and Ryan Cotterell. Generalizing backpropagation for gradient-based interpretability. *arXiv preprint arXiv:2307.03056*, 2023.
- [10] Mehdi Fatemi, Banafsheh Rafiee, Mingjie Tang, and Kartik Talamadupula. Concise reasoning via reinforcement learning. *arXiv preprint arXiv:2504.05185*, 2025.
- [11] Sam Glucksberg and Matthew S McGlone. *Understanding figurative language: From metaphor to idioms*. Number 36. Oxford University Press, 2001.
- [12] Arthur C Graesser, Murray Singer, and Tom Trabasso. Constructing inferences during narrative text comprehension. *Psychological review*, 101(3):371, 1994.
- [13] Daya Guo, Dejian Yang, Haowei Zhang, Junxiao Song, Ruoyu Zhang, Runxin Xu, Qihao Zhu, Shirong Ma, Peiyi Wang, Xiao Bi, et al. Deepseek-r1: Incentivizing reasoning capability in llms via reinforcement learning. *arXiv preprint arXiv:2501.12948*, 2025.
- [14] Shibo Hao, Sainbayar Sukhbaatar, DiJia Su, Xian Li, Zhiting Hu, Jason Weston, and Yuandong Tian. Training large language models to reason in a continuous latent space. *arXiv preprint arXiv:2412.06769*, 2024.
- [15] Dan Hendrycks, Collin Burns, Saurav Kadavath, Akul Arora, Steven Basart, Eric Tang, Dawn Song, and Jacob Steinhardt. Measuring mathematical problem solving with the math dataset. *NeurIPS*, 2021.
- [16] Edward J Hu, yelong shen, Phillip Wallis, Zeyuan Allen-Zhu, Yuanzhi Li, Shean Wang, Lu Wang, and Weizhu Chen. LoRA: Low-rank adaptation of large language models. In *International Conference on Learning Representations*, 2022. URL <https://openreview.net/forum?id=nZeVKeeFYf9>.
- [17] Aaron Jaech, Adam Kalai, Adam Lerer, Adam Richardson, Ahmed El-Kishky, Aiden Low, Alec Hel-lyar, Aleksander Madry, Alex Beutel, Alex Carney, et al. Openai o1 system card. *arXiv preprint arXiv:2412.16720*, 2024.
- [18] Daniel Kahneman. *Thinking, fast and slow*. macmillan, 2011.
- [19] Yu Kang, Xianghui Sun, Liangyu Chen, and Wei Zou. C3ot: Generating shorter chain-of-thought without compromising effectiveness. In *Proceedings of the AAAI Conference on Artificial Intelligence*, volume 39, pages 24312–24320, 2025.
- [20] Andrew Karpinski and James L Hilton. Attitudes and the implicit association test. *Journal of personality and social psychology*, 81(5):774, 2001.
- [21] Angelos Katharopoulos, Apoorv Vyas, Nikolaos Pappas, and François Fleuret. Transformers are rnns: Fast autoregressive transformers with linear attention. In *International conference on machine learning*, pages 5156–5165. PMLR, 2020.
- [22] Tengxiao Liu, Qipeng Guo, Xiangkun Hu, Cheng Jiayang, Yue Zhang, Xipeng Qiu, and Zheng Zhang. Can language models learn to skip steps? *arXiv preprint arXiv:2411.01855*, 2024.

- [23] Haotian Luo, Li Shen, Haiying He, Yibo Wang, Shiwei Liu, Wei Li, Naiqiang Tan, Xiaochun Cao, and Dacheng Tao. O1-pruner: Length-harmonizing fine-tuning for o1-like reasoning pruning. *arXiv preprint arXiv:2501.12570*, 2025.
- [24] Wenjie Ma, Jingxuan He, Charlie Snell, Tyler Griggs, Sewon Min, and Matei Zaharia. Reasoning models can be effective without thinking. *arXiv preprint arXiv:2504.09858*, 2025.
- [25] Niklas Muennighoff, Zitong Yang, Weijia Shi, Xiang Lisa Li, Li Fei-Fei, Hannaneh Hajishirzi, Luke Zettlemoyer, Percy Liang, Emmanuel Candès, and Tatsunori Hashimoto. s1: Simple test-time scaling. *arXiv preprint arXiv:2501.19393*, 2025.
- [26] Zhuoshi Pan, Qianhui Wu, Huiqiang Jiang, Menglin Xia, Xufang Luo, Jue Zhang, Qingwei Lin, Victor Rühle, Yuqing Yang, Chin-Yew Lin, et al. Llm-lingua-2: Data distillation for efficient and faithful task-agnostic prompt compression. *arXiv preprint arXiv:2403.12968*, 2024.
- [27] Judea Pearl et al. Models, reasoning and inference. *Cambridge, UK: CambridgeUniversityPress*, 19(2):3, 2000.
- [28] Xiaoye Qu, Yafu Li, Zhaochen Su, Weigao Sun, Jianhao Yan, Dongrui Liu, Ganqu Cui, Daizong Liu, Shuxian Liang, Junxian He, et al. A survey of efficient reasoning for large reasoning models: Language, multimodality, and beyond. *arXiv preprint arXiv:2503.21614*, 2025.
- [29] Anton Razzhigaev, Matvey Mikhalchuk, Temurbek Rahmatullaev, Elizaveta Goncharova, Polina Druzhinina, Ivan Oseledets, and Andrey Kuznetsov. Llm-microscope: Uncovering the hidden role of punctuation in context memory of transformers. *arXiv preprint arXiv:2502.15007*, 2025.
- [30] David Rein, Betty Li Hou, Asa Cooper Stickland, Jackson Petty, Richard Yuanzhe Pang, Julien Dirani, Julian Michael, and Samuel R Bowman. Gpqa: A graduate-level google-proof q&a benchmark. In *First Conference on Language Modeling*, 2024.
- [31] Paul R Rosenbaum and Donald B Rubin. The central role of the propensity score in observational studies for causal effects. *Biometrika*, 70(1):41–55, 1983.
- [32] Donald B Rubin. Causal inference using potential outcomes: Design, modeling, decisions. *Journal of the American statistical Association*, 100(469):322–331, 2005.
- [33] Nikunj Saunshi, Nishanth Dikkala, Zhiyuan Li, Sanjiv Kumar, and Sashank J Reddi. Reasoning with latent thoughts: On the power of looped transformers. *arXiv preprint arXiv:2502.17416*, 2025.
- [34] Noam Shazeer, Azalia Mirhoseini, Krzysztof Maziarz, Andy Davis, Quoc Le, Geoffrey Hinton, and Jeff Dean. Outrageously large neural networks: The sparsely-gated mixture-of-experts layer. *arXiv preprint arXiv:1701.06538*, 2017.
- [35] Yi Shen, Jian Zhang, Jieyun Huang, Shuming Shi, Wenjing Zhang, Jiangze Yan, Ning Wang, Kai Wang, and Shiguo Lian. Dast: Difficulty-adaptive slow-thinking for large reasoning models. *arXiv preprint arXiv:2503.04472*, 2025.
- [36] Amitai Shenhav, Matthew M Botvinick, and Jonathan D Cohen. The expected value of control: an integrative theory of anterior cingulate cortex function. *Neuron*, 79(2):217–240, 2013.
- [37] Avanti Shrikumar, Peyton Greenside, and Anshul Kundaje. Learning important features through propagating activation differences. In *International conference on machine learning*, pages 3145–3153. PMLR, 2017.
- [38] Keith E Stanovich, Richard F West, and JE Alder. Individual differences in reasoning: Implications for the rationality debate?-open peer commentary-three fallacies. *Behavioral and Brain Sciences*, 23(5):665–665, 2000.
- [39] DiJia Su, Sainbayar Sukhbaatar, Michael Rabbat, Yuandong Tian, and Qingqing Zheng. Dualformer: Controllable fast and slow thinking by learning with randomized reasoning traces. In *The Thirteenth International Conference on Learning Representations*, 2024.
- [40] Yang Sui, Yu-Neng Chuang, Guanchu Wang, Jiamu Zhang, Tianyi Zhang, Jiayi Yuan, Hongyi Liu, Andrew Wen, Hanjie Chen, Xia Hu, et al. Stop overthinking: A survey on efficient reasoning for large language models. *arXiv preprint arXiv:2503.16419*, 2025.
- [41] Mukund Sundararajan, Ankur Taly, and Qiqi Yan. Axiomatic attribution for deep networks. In *International conference on machine learning*, pages 3319–3328. PMLR, 2017.

- [42] Gemma Team, Aishwarya Kamath, Johan Ferret, Shreya Pathak, Nino Vieillard, Ramona Merhej, Sarah Perrin, Tatiana Matejovicova, Alexandre Ramé, Morgane Rivière, et al. Gemma 3 technical report. *arXiv preprint arXiv:2503.19786*, 2025.
- [43] Amos Tversky and Daniel Kahneman. Judgment under uncertainty: Heuristics and biases: Biases in judgments reveal some heuristics of thinking under uncertainty. *science*, 185(4157):1124–1131, 1974.
- [44] Ashish Vaswani, Noam Shazeer, Niki Parmar, Jakob Uszkoreit, Llion Jones, Aidan N Gomez, Łukasz Kaiser, and Illia Polosukhin. Attention is all you need. *Advances in neural information processing systems*, 30, 2017.
- [45] Xinglin Wang, Shaoxiong Feng, Yiwei Li, Peiwen Yuan, Yueqi Zhang, Chuyi Tan, Boyuan Pan, Yao Hu, and Kan Li. Make every penny count: Difficulty-adaptive self-consistency for cost-efficient reasoning. *arXiv preprint arXiv:2408.13457*, 2024.
- [46] Yongjie Wang, Tong Zhang, Xu Guo, and Zhiqi Shen. Gradient based feature attribution in explainable ai: A technical review. *arXiv preprint arXiv:2403.10415*, 2024.
- [47] Jason Wei, Xuezhi Wang, Dale Schuurmans, Maarten Bosma, Fei Xia, Ed Chi, Quoc V Le, Denny Zhou, et al. Chain-of-thought prompting elicits reasoning in large language models. *Advances in neural information processing systems*, 35:24824–24837, 2022.
- [48] Heming Xia, Yongqi Li, Chak Tou Leong, Wenjie Wang, and Wenjie Li. Tokenskip: Controllable chain-of-thought compression in llms. *arXiv preprint arXiv:2502.12067*, 2025.
- [49] An Yang, Baosong Yang, Beichen Zhang, Binyuan Hui, Bo Zheng, Bowen Yu, Chengyuan Li, Dayiheng Liu, Fei Huang, Haoran Wei, et al. Qwen2. 5 technical report. *arXiv preprint arXiv:2412.15115*, 2024.
- [50] Wenkai Yang, Shuming Ma, Yankai Lin, and Furu Wei. Towards thinking-optimal scaling of test-time compute for llm reasoning. *arXiv preprint arXiv:2502.18080*, 2025.
- [51] Yixin Ye, Zhen Huang, Yang Xiao, Ethan Chern, Shijie Xia, and Pengfei Liu. Limo: Less is more for reasoning. *arXiv preprint arXiv:2502.03387*, 2025.
- [52] Edward Yeo, Yuxuan Tong, Morry Niu, Graham Neubig, and Xiang Yue. Demystifying long chain-of-thought reasoning in llms. *arXiv preprint arXiv:2502.03373*, 2025.

## A Detailed Experimental Setup

This appendix provides comprehensive details regarding the experimental setup, supplementing the information presented in Section 4.1.

### A.1 Training Data Source and Pre-processing

**Data Source** We utilize the MATH training dataset [48], specifically its canonical subset comprising 7,500 question-answer pairs. Each pair includes a problem statement, a reference Chain-of-Thought (CoT) solution, and the ground truth answer.

**CoT and Answer Extraction** We systematically extract the CoT reasoning from the provided solution field using rigorous pattern matching techniques targeting the standard `answer` format demarcation, thereby separating the reasoning path from the final solution.

**Validation Protocol** We verify the mathematical equivalence of extracted answers against ground truth values using a symbolic mathematics library and retain only samples where the extracted answer is symbolically equivalent to the ground truth (strict equivalence). We tokenize all CoTs using model-specific tokenizers before further processing. Samples exhibiting excessive token length (>1,500 tokens) or causing computational infeasibility during GoGI calculation are excluded. This filtering process yields the final dataset of 7,472 valid samples used for training data generation.

### A.2 GoGI Target Layer Selection Justification

**Analysis Methodology and Rationale** The target layer  $l^*$  for GoGI calculation significantly impacts the captured importance signals. Since computing GoGI scores across all layers is computationally prohibitive, we employ a layer contribution analysis as an efficient proxy to guide the selection of a single, representative target layer  $l^*$  for each model. This analysis computes, for each layer  $l$ , the average L1 norm of the gradients propagated from the top-1 prediction logit (at each valid CoT position  $t$ ) back to the input activation  $\mathbf{x}_t^l$  of that layer’s MLP down-projection module (see Algorithm 1 for details). This metric reflects the layer’s processing intensity related to local predictions. We hypothesize that layers exhibiting high contribution in this analysis are crucial for information integration and likely contain intermediate representations  $\mathbf{h}_t^l$  that are highly sensitive to the final answer loss, making them suitable candidates for GoGI calculation. This analysis is less computationally intensive than full GoGI calculation and thus allows us to identify promising candidate regions for  $l^*$ .

**Cross-Model Observations and Layer Selection** Figure 5 presents the layer-wise contribution distributions for all evaluated models and reveals significant diversity across architectures and scales. While Gemma models (1B, 4B, 12B) tend to show increasing contributions that peak in the latter middle-to-late stages, Qwen models exhibit different patterns. Qwen2.5-7B shows a remarkably early peak, followed by a steep decline then a minor secondary peak, while Qwen2.5-3B displays a broader peak region centered around L17-18. Gemma-1B also presents a simpler profile with a single primary peak zone.

This heterogeneity suggests that a universal, optimal relative depth for  $l^*$  likely does not exist. Different models seem to employ different layer specialization strategies for processing information within CoT. However, despite these varied contribution profiles, our preliminary experiments indicated that the final reasoning accuracy of Adaptive GoGI-Skip was not highly sensitive to the precise choice of  $l^*$ , as long as we selected a layer with reasonably high contribution. Choosing a layer with near-zero contribution (e.g., the very first or very last layers) significantly degraded performance, but variations among several high-contribution layers yielded comparable results. This observed robustness, despite varying contribution profiles, might stem from several factors: (1) The relative ranking of token importance derived from GoGI scores may be reasonably preserved across several suitable mid-to-late layers, despite variations in absolute score magnitudes. (2) The ADS mechanism—particularly EDR, which normalizes entropy signals, and ANC, which provides coherence safety—might compensate for some level of suboptimality in the raw GoGI signals. (3) The SFT process itself enables the model to adapt to the specific importance signals derived from the chosen  $l^*$ .

---

**Algorithm 1:** Layer Contribution Calculation for a Single Sample.

---

**Input** : Model  $M_\theta$ , Tokenizer  $T$ , Sample  $s = (problem, cot, answer)$ , CoT Token IDs  $c_{ids}$   
**Output** : Per-layer average contributions for sample  $s$ :  $Contrib_s = \{l : avg\_contrib_l\}$   
 $L \leftarrow$  Number of layers in  $M_\theta$   
 $LayerGrads \leftarrow \{\}$  for  $l = 0$  to  $L - 1$   
 $Hooks \leftarrow$  RegisterBackwardHook(on MLP down\_proj input for all layers  $l$ , capturing gradients into  $LayerGrads$ )  
 $InputText \leftarrow$  FormatInput( $T, s.problem, s.cot, s.answer$ )  
 $InputIDs \leftarrow T(InputText)$   
 $cot\_idx\_range \leftarrow$  GetCoTIndices( $c_{ids}, InputIDs$ )  
**if**  $cot\_idx\_range = NotFound$  **then**  
| **return**  $\emptyset$   
**end**  
 $HiddenStates, Logits \leftarrow M_\theta(InputIDs, output\_hidden\_states=True)$   
 $SampleLC \leftarrow \{\}$  for  $l = 0$  to  $L - 1$   
**foreach** token index  $t$  from  $cot\_idx\_range.start$  to  $cot\_idx\_range.end - 1$  **do**  
| **if**  $t < Logits.shape[1] - 1$  **then**  
| |  $LayerGrads \leftarrow \emptyset$   
| |  $M_\theta.zero\_grad()$   
| |  $target\_logit \leftarrow Logits[0, t]$   
| |  $pred\_id \leftarrow \text{argmax}(target\_logit)$   
| |  $grad\_output \leftarrow \text{OneHot}(pred\_id)$   
| |  $target\_logit.backward(grad\_output, retain\_graph=True)$   
| | **foreach** layer  $l$  from 0 to  $L - 1$  **do**  
| | | **if**  $l$  in  $LayerGrads$  **then**  
| | | | Append  $\mathbb{L}1NormLayerGrads[l]$  to  $SampleLC[l]$   
| | | **end**  
| | **end**  
| **end**  
**end**  
 $Contrib_s \leftarrow \{\}$   
**foreach** layer  $l$  in  $SampleLC$  **do**  
| **if**  $SampleLC[l]$  is not empty **then**  
| |  $Contrib_s[l] \leftarrow \text{mean}(SampleLC[l])$   
| **end**  
**end**  
**return**  $Contrib_s$

---

**Selection Principle and Final Layers** Given the observed robustness and the clear variance in peak locations, we adopted the following pragmatic selection principle: identify the layer(s) exhibiting the latest visually significant peak or plateau in the gradient contribution analysis plot (determined via inspection of distributions like those in Figure 5). We generally prefer later layers within this candidate set, as they likely capture more integrated semantic understanding relevant to the final answer while still possessing strong discriminative signals before potential output layer saturation effects. Based on this principle, we selected the following target layers  $l^*$  for GoGI computation; Table 4 illustrates these selections.

Table 4: **Target Layer ( $l^*$ ) Selection for GoGI Computation.** Selected layers are based on observed gradient contribution peaks across different models.

Model Name	Layer Size	Selected Layer ( $l^*$ )
Gemma-3-1B-it	26	18
Gemma-3-4B-it	34	23
Gemma-3-12B-it	48	35
Qwen2.5-3B-it	36	18
Qwen2.5-7B-it	40	27

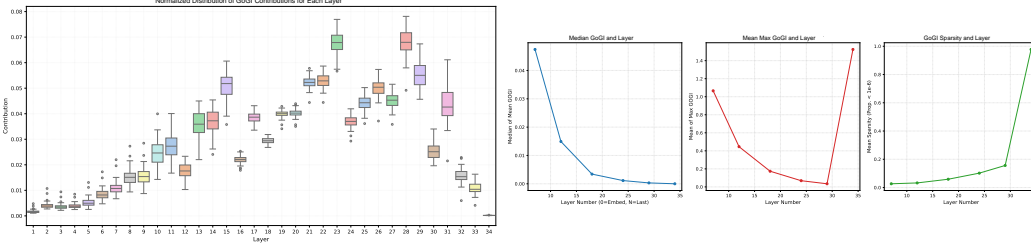


Figure 4: **Analysis supporting GoGI target layer selection for Gemma3-4B-it.** **Left:** Layer-wise gradient contribution to logits. **Right:** GoGI statistics across layers. While high max GoGI occurs near L23 and L28, L23 shows stronger overall contribution, which informs our choice.

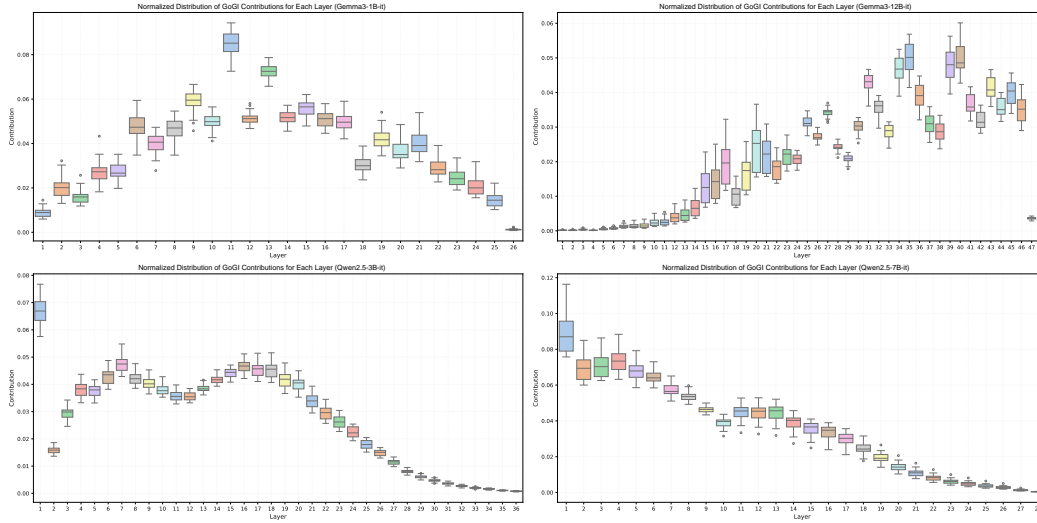


Figure 5: **Distribution of normalized gradient contributions from each layer to the final logits across all evaluated models.** **Top:** Gemma3-1B-it and Gemma3-12B-it. **Bottom:** Qwen2.5-1B-it and Qwen2.5-7B-it.

These selections represent a consistent strategy based on empirical observation of contribution peaks and aim for layers rich in processed, task-relevant information.

### A.3 Adaptive GoGI-Skip Hyperparameters and Algorithmic Details

To enhance the robustness and potentially reduce the need for extensive manual hyperparameter tuning across different datasets or model initializations, our framework includes an optional **Adaptive Parameter Tuner** module, which we utilize during the initial phases of data processing or exploration. This appendix details its mechanism and other relevant algorithmic details.

**Motivation** The optimal settings for ADS hyperparameters, such as the base retention rate ( $\gamma_{base}$ ), entropy scaling factors ( $s_\gamma, s_N$ ), or N-constraint bounds ( $N_{min}, N_{max}$ ), might ideally depend on the overall statistical properties of the dataset being processed (e.g., average CoT length, typical entropy range, GoGI score distribution). The Adaptive Parameter Tuner aims to adjust these parameters automatically based on features extracted from an initial subset of the data.

The Tuner operates in three main steps:

- **Data Feature Analysis:** The tuner first processes a small subset of the input data to compute various statistical features (e.g., average CoT length, entropy distribution moments).
- **Optimal Target Ratio Estimation:** Based on these extracted features, the tuner employs a predefined heuristic function (details omitted) to estimate a recommended overall target compression ratio ( $\gamma_{target}$ ) for the entire dataset. This function typically considers factors

like entropy distribution (higher average entropy or variance might suggest more conservative compression). This estimated  $\gamma_{target}$  then serves as a reference for subsequent parameter adjustments.

- **Parameter Update:** Based on the extracted features and the estimated  $\gamma_{target}$ , the tuner then adjusts key ADS hyperparameters (specifically, those marked with () in Table 5, such as  $\gamma_{base}$ ,  $s_\gamma$ ,  $s_N$ ,  $N_{min}$ ,  $N_{max}$ ) using internal heuristics (details omitted).

Table 5 lists the key default hyperparameters used for the ADS mechanism.

Table 5: **Comprehensive Hyperparameter Configuration for Adaptive GoGI-Skip Mechanism.** Parameters marked with () are dynamically estimated (e.g.,  $H_{median}$ ,  $H_{std}$ ) or adjusted (e.g.,  $\gamma_{base}$ ,  $N_{max}$ ) by the *Adaptive Parameter Tuner* based on dataset-specific characteristics.

Parameter	Symbol	Default
<b>EDR Regulation</b>		
Min Retention Rate	$\gamma_{min}$	0.2
Max Retention Rate	$\gamma_{max}$	0.8
Base Gamma	$\gamma_{base}$	0.6
Entropy Delta	$\delta_e$	0.3
Entropy Scale Factor	$s_\gamma$	1.8
Entropy Mapping Mode	$mode$	auto
Entropy Median	$H_{median}$	Estimated
Entropy Std Dev	$H_{std}$	Estimated
<b>ANC Coherence</b>		
Min Consecutive Skips	$N_{min}$	1
Max Consecutive Skips	$N_{max}$	9
Entropy Window Size	$W$	9
Entropy Scale Factor	$s_N$	1.8
<b>Token Filtering &amp; Weighting</b>		
Ignored Token IDs	$\mathcal{I}_{ignore}$	Space ID
Token Type Weighting	$w_t$	Enabled

**Token Filtering for Threshold Calculation ( $\mathcal{I}_{valid}$ )** When calculating the dynamic GoGI threshold  $\tau_t$  (Eq. 6), the percentile is computed over the GoGI scores of tokens belonging to the index set  $\mathcal{I}_{valid}$ . By default,  $\mathcal{I}_{valid}$  excludes tokens classified as 'Space' to prevent common, low-GoGI space tokens from skewing the percentile calculation. Other specific special tokens or punctuation marks can also be excluded depending on the specific configuration used.

**Entropy Mapping Functions ( $\mathcal{M}, \mathcal{M}'$ )** The mapping functions  $\mathcal{M}$  and  $\mathcal{M}'$ , employed in Equations 5 and 9 respectively, normalize entropy values based on estimated global statistics ( $H_{median}$ ,  $H_{std}$ ) and apply a selected transformation (modes: auto, sigmoid, tanh, gaussian, piecewise). The 'auto' mode selects a suitable transformation based on the estimated standard deviation of entropy ( $H_{std}$ ) to improve robustness across different distributions. Scale factors ( $s_\gamma$ ,  $s_N$ ) control the sensitivity (slope) of the mapping.

#### A.4 Hardware, Software, and Constraints

**Computational Infrastructure** We conducted all experiments on a high-performance computing server equipped with  $3 \times$  NVIDIA GeForce RTX 4090 GPUs, each providing 24GB of VRAM for parallel computation tasks.

**Software Environment** Our experimental software stack comprised Python 3.12.9, PyTorch 2.6, Transformers 4.51.3, and CUDA 12.4, ensuring compatibility and optimal performance across all computational tasks.

**GoGI Computation Constraints and Cost** Due to the nature of GoGI score calculation requiring independent backpropagation per sample for precise answer-loss gradients, efficient multi-GPU

parallelization for the gradient calculations proved challenging on our specific hardware (RTX 4090 lacks NVLink, potentially hindering certain gradient synchronization strategies). To ensure gradient accuracy, we computed GoGI scores using a single RTX 4090 with unquantized models. The offline GoGI calculation for the 7,472 MATH training samples on the Gemma-3-4B-it model required approximately 12 GPU hours on a single GPU. The subsequent dynamic compression step, including entropy calculation and pruning logic, took an additional 16 GPU hours (approx. 8h entropy, 8h pruning) on a single GPU. We store pre-estimated entropy statistics ( $H_{\text{median}}, H_{\text{std}}$ ), allowing parameter adjustments without full re-computation. While representing a significant one-time offline cost per dataset/model, this compute budget is often comparable to or less than that required for extensive hyperparameter sweeps or typical Reinforcement Learning from Human Feedback (RLHF) / RL-based optimization processes.

### A.5 SFT and LoRA Hyperparameters

**SFT and LoRA Hyperparameters** We performed supervised fine-tuning for all methods requiring it (including Adaptive GoGI-Skip, TokenSkip, C3ot-like, and Spiritft) using Parameter-Efficient Fine-Tuning (PEFT) with the Low-Rank Adaptation (LoRA) technique [16]. Table 6 lists the typical hyperparameters we used across models. Minor adjustments may have been made based on model size and convergence observations during initial runs.

Table 6: **Typical LoRA SFT Hyperparameters.**

Parameter	Value(s)
LoRA Rank ( $r$ )	16 (for 1B/3B), 32 (for 4B/7B/12B)
LoRA Alpha ( $\alpha$ )	32 (for 1B/3B), 64 (for 4B/7B/12B)
LoRA Dropout	0.05
Target Modules	$q_{proj}, k_{proj}, v_{proj}, o_{proj}$
Learning Rate	$2e-5$
Batch Size (per device)	1-8 (adjusted based on model size and GPU memory)
Gradient Accumulation Steps	Adjusted to achieve effective batch size of 64-128
Number of Epochs	1-2
LR Scheduler	cosine
Warmup Ratio	0.03
Optimizer	AdamW ( <code>adamw_torch</code> )
Mixed Precision	BF16

### A.6 Latency and Speedup Measurements

To provide a consistent and fair comparison of inference efficiency, we conducted all latency measurements on a standardized hardware setup and under controlled conditions.

**Hardware Configuration** We measured latency for all models and methods on a single NVIDIA GeForce RTX 4090 GPU with 24GB VRAM. This ensures that reported speedups are not confounded by differences in computational resources.

**Inference Batch Size** We used a batch size of 1 for all latency measurements. This reflects a common real-world scenario for interactive or single-query reasoning tasks and provides a measure of per-sample processing time without batching amortization.

**Decoding Strategy** Consistent with our accuracy evaluations, we employed greedy decoding (temperature set to 0.0 where applicable, or `top-p=1.0, do sample=False`) for all latency tests to ensure deterministic output lengths for a given input and method.

**Warm-up** Before formal latency measurement for each model/method configuration on a benchmark, we performed a small number of warm-up inference runs (100 samples). This helps mitigate the impact of initial model loading times, CUDA kernel compilation, or other one-time setup costs on the measured latency.

**Measurement Protocol** For each (model, method, benchmark) combination, we measured the end-to-end inference time for each sample in the test set. This included the time from receiving the input prompt to generating the complete CoT and final answer. We then calculated the average per-sample latency by dividing the total time taken for all samples in a benchmark by the number of samples.

**Repetitions and Averaging** To account for minor system fluctuations, we typically averaged the latency measurement for each benchmark over 2-3 complete passes through the test set, or a sufficiently large subset if the full set was too time-consuming for multiple passes. The reported average latency is the mean across these passes.

**Speedup Calculation** We calculate the Latency Speedup reported in our main results tables as the ratio of the average per-sample latency of the Original (uncompressed) model to the average per-sample latency of the evaluated compression method on the same benchmark and base model:

$$\text{Speedup}_{\text{Method}} = \frac{\text{AvgLatency}_{\text{Original}}}{\text{AvgLatency}_{\text{Method}}} \quad (11)$$

This detailed protocol aims to provide robust and comparable latency and speedup figures, reflecting the practical efficiency gains of Adaptive GoGI-Skip.

## B Baseline Implementation Details

This appendix elaborates on the implementation specifications for the baseline methods used in our comparative evaluation (Section 4). To ensure methodological rigor, we trained all SFT-based baselines (C3ot, Spiritft, TokenSkip) on compressed CoT data generated using their respective methodologies, as detailed below. This data was derived from the identical 7,472 validated MATH training samples used to generate training data for Adaptive GoGI-Skip, thereby facilitating a direct comparison of the underlying compression strategies.

For the C3ot baseline, we used greedy decoding with the compressor model (Gemma-3-4B-it) to generate the compressed CoT for each training sample based on the prompt. For the Spiritft and TokenSkip baselines, we applied their respective offline pruning algorithms (detailed below for Spiritft, see Section B.4 for TokenSkip) to the original CoTs to create the compressed training data. We then used these resulting compressed datasets (each containing `< problem, compressed CoT, answer >` triplets specific to a baseline method) to fine-tune all target models (Gemma 1B/4B/12B, Qwen 3B/7B) via LoRA SFT, following the identical LoRA SFT procedure (detailed in Appendix A.5) used for Adaptive GoGI-Skip.

### B.1 C3ot

**C3ot.** To establish a baseline reflecting compression guided by a capable language model without reliance on external proprietary APIs, we implemented a self-compression strategy inspired by C3ot [19]. Specifically, we employed our primary analysis model (`google/gemma-3-4b-it`) as the compression agent. For each of the 7,472 validated source CoT samples (`problem, original_cot, answer`), we instructed this Gemma-3-4B-it model to generate a condensed version of the original CoT (`original_cot`) using the following prompt template:

### C3ot Compression Prompt Template

You will be given a detailed step-by-step reasoning process used to solve a math problem. Your task is to significantly compress this reasoning process while preserving all critical logical steps, and the final conclusion necessary to arrive at the correct answer. Eliminate redundant explanations, repetitive phrasing, trivial arithmetic steps, and verbose language. The compressed reasoning should be clear, logically sound, and contain enough information for someone knowledgeable to verify the solution path. Output ONLY the compressed reasoning process.

## Original Reasoning:  
{original cot}

## Compressed Reasoning:

## B.2 Prompting

**Prompting.** This baseline represents a zero-shot approach involving no fine-tuning. Instead, we directly instructed the original base models during inference to generate more concise reasoning traces. We experimented with several prompt variations aiming for conciseness. The template yielding a reasonable balance between conciseness and task completion, which we used for the results reported in Section 4, is shown below. We prepended this prompt to the standard problem input for each model.

### Prompting Compression Prompt Template

Please provide a concise step-by-step solution to the following problem. Focus only on the essential calculations and logic needed to reach the answer. Avoid verbose explanations or stating obvious facts. Put your final answer within `\boxed{answer}`.

## Problem:  
{problem}

## Solution:

As observed in prior work [48] and confirmed in ours, while this zero-shot prompting approach sometimes slightly reduced verbosity compared to standard CoT prompting, it often led to incomplete reasoning or significant accuracy degradation. This highlights the limitations of relying solely on zero-shot instructions for complex CoT modification tasks.

## B.3 Spiritft

**Spiritft.** To evaluate compression approaches based on predictability metrics (as opposed to goal-oriented importance), we implemented a static pruning baseline inspired by Spiritft [7], specifically adapted for offline SFT data generation. The core Spiritft methodology identifies expendable reasoning steps by analyzing changes in perplexity upon step removal. Our implementation proceeded through the following systematic stages:

1. **Reasoning Segmentation:** We decomposed each source CoT from the 7,472 MATH samples into discrete reasoning steps  $(s_1, s_2, \dots, s_N)$ . We primarily employed sentence boundaries (periods followed by spaces or newlines) as primary delimiters, supplemented by heuristics to handle common mathematical notation and formatting variations (e.g., preserving lines with equations).
2. **Step Importance Quantification:** We quantified the importance of each step  $s_j$  by measuring the impact of its omission on the base model’s processing fluency. For each step  $s_j$ , we constructed a pruned CoT  $c'_j = s_1 \dots s_{j-1} s_{j+1} \dots s_N$ . We then calculated the resulting increase in average negative log-likelihood ( $\Delta\text{NLL}(s_j)$ ) incurred when the original base

model (corresponding to the 'Original' baseline) processed  $c'_j$  compared to processing the original sequence  $c$ . Lower  $\Delta\text{NLL}$  values signify lower step importance.

3. **Retention-Based Pruning:** We applied static pruning based on a target retention ratio  $\gamma$ . Specifically, we retained the  $\lceil \gamma \cdot N \rceil$  steps exhibiting the highest  $\Delta\text{NLL}$  values (i.e., deemed most essential by this predictability metric) and discarded the rest. We calibrated  $\gamma$  for Spiritft by selecting values that resulted in average compression ratios on the training set closely matching those of the TokenSkip baseline variants (i.e., targeting average ratios around 0.5 and 0.6) to ensure equitable comparison.
4. **Sequence Reconstruction:** To preserve basic coherence after pruning, we simply concatenated the retained steps in their original sequential order. We deliberately omitted the semantic merging step described in the original SpiritFT methodology [7] (which handles cases where removal might impair coherence) to specifically isolate the evaluation to the effectiveness of the core perplexity-based importance assessment for pruning.

We subsequently used the resulting dataset (containing `< problem, perplexity-pruned CoT, answer >` triplets) for LoRA SFT of all target models. This setup enabled a direct comparison between our GoGI-based importance scoring and this established predictability-based approach within a comparable static compression framework.

#### B.4 TokenSkip

**TokenSkip.** The TokenSkip SFT baseline [48] requires offline generation of training data compressed to specific target retention ratios ( $\gamma = 0.5$  and  $\gamma = 0.6$ , matching our evaluation settings). We generated two separate datasets using the LLMingua library [26] as follows:

1. We initialized the `llmlingua.PromptCompressor` with the recommended `llmlingua-2-xml-roberta-large` model [6].
2. For each original CoT in the 7,472 validated samples, we used the `compress_prompt` method to compress the CoT text.
3. We set the target rate parameter in `compress_prompt` to  $\gamma$ . Additional library parameters were used as detailed in the code release, aiming to preserve essential operators.
4. The `compressed_prompt` output from LLMingua served as the compressed CoT for the corresponding SFT training dataset (one dataset generated for  $\gamma = 0.5$ , one for  $\gamma = 0.6$ ).

This procedure directly employed the LLMingua tool to create static compressed datasets based on its internal importance metrics and compression algorithm at the specified target ratios.

### C Detailed Token Retention Analysis by Functional Type

To further elucidate the pruning behavior of Adaptive GoGI-Skip relative to baseline methods, we analyzed average token retention rates across different functional token categories on the MATH Test dataset using Gemma-3-4B-it. These categories classify tokens based on linguistic and mathematical roles.

Table 7 presents the retention rates per category. Adaptive GoGI-Skip exhibits a highly discriminative profile: it achieves the highest retention for Numerals (93.1%), Operators (91.3%), and Symbols (88.2%). This confirms that its GoGI metric, particularly when enhanced by the type-weighting strategy employed in our experiments, effectively identifies and preserves tokens essential for mathematical logic and computation. Such high retention of core mathematical elements contrasts sharply with methods like TokenSkip, for instance, TokenSkip ( $\gamma = 0.5$ ) retains only 75.2% of Numerals.

At the other extreme, Adaptive GoGI-Skip demonstrates high effectiveness in removing General Language tokens (23.7% retention)—a category encompassing common words not classified elsewhere and representing the bulk of compressible text. This rate is markedly lower than those achieved by other evaluated methods, indicating a highly targeted pruning of descriptive or narrative text with low functional relevance to the core reasoning steps. For intermediate categories like Formatting (60.5% retention) and Connectives (55.0% retention), Adaptive GoGI-Skip maintains a balanced approach. This pattern suggests that while many tokens in these categories are pruned, a subset

Table 7: Average Token Retention Rate (%) by Functional Type on the MATH Test dataset (Model: Gemma-3-4B-it).

Method	Numerals	Operators	Symbols	Formatting	Connectives	General	Overall
Prompting	95.5	94.2	93.7	88.3	85.9	82.5	0.91
C3ot	84.1	82.8	79.5	63.4	58.2	48.6	0.67
Spiritft	80.3	78.5	75.8	56.2	51.6	40.8	0.65
TokenSkip ( $\gamma = 0.6$ )	81.3	79.2	76.5	58.0	53.1	38.5	0.63
TokenSkip ( $\gamma = 0.5$ )	75.2	72.4	70.1	48.5	44.6	30.9	0.55
<b>Adaptive GoGI-Skip</b>	93.1	91.3	88.2	60.5	55.0	23.7	0.52

deemed critical for coherence—plausibly preserved by the ANC mechanism overriding low GoGI scores, or assigned sufficiently high weighted GoGI scores initially—is retained more effectively than occurs with purely aggressive static methods like TokenSkip ( $\gamma = 0.5$ ). For instance, the aggressive TokenSkip ( $\gamma = 0.5$ ) baseline reduces Formatting and Connectives retention to only 48.5% and 44.6%, respectively.

The remaining baselines exhibit different profiles. The C3ot baseline retains considerably more General Language (48.6%) and Formatting (63.4%) tokens than Adaptive GoGI-Skip, suggesting less targeted pruning of non-essential text. The Spiritft baseline’s retention profile generally falls between TokenSkip’s conservative ( $\gamma = 0.6$ ) and aggressive ( $\gamma = 0.5$ ) settings. Finally, as expected, the Prompting baseline exhibits very high retention across all categories, which reflects its overall inefficiency.

In summary, this detailed analysis of token retention by functional type provides compelling evidence that Adaptive GoGI-Skip achieves highly targeted and functionally aware compression. Specifically, the high retention of mathematical tokens supports the effectiveness of the GoGI metric, while the balanced handling of structural/connective tokens suggests the ANC mechanism successfully preserves coherence. This demonstrably targeted compression approach directly contributes to the method’s superior efficiency-accuracy balance.

## D Detailed Analysis of Goal-Gradient Importance Scores

This appendix presents a comprehensive analysis of GoGI scores, extending the distributional analysis in Section 4.3 (Figure 2). We investigate relationships between GoGI scores and external factors (CoT length, problem difficulty) as well as internal model metrics (predictive entropy). All analyses utilize GoGI scores computed at the selected target layer  $l^*$  (see Section A.2) for the 7,472 validated MATH training samples using the Gemma-3-4B-it model.

### D.1 Relationship Between GoGI and External Problem Characteristics

To assess if GoGI scores merely reflect superficial sequence properties, we first systematically investigated their relationship with external problem characteristics: CoT length and problem difficulty level (visualized in Figure 6).

The scatter plot analysis (Figure 6, top) reveals that Mean GoGI scores exhibit only a weak negative correlation with CoT length (Spearman’s  $r_s \approx -0.15$ ,  $p < 0.01$ ), suggesting minimal impact from sequence length on average token importance. More significantly, Maximum GoGI scores show negligible correlation with sequence length ( $|r_s| < 0.05$ , n.s.), indicating that the occurrence of highly critical tokens is independent of overall reasoning chain length.

Turning to problem difficulty, the difficulty-stratified analysis (Figure 6, bottom) reveals no statistically significant monotonic relationship between GoGI metrics and MATH problem difficulty levels. Although higher difficulty problems exhibit slightly increased variance in their GoGI distributions, median importance values remain remarkably consistent across difficulty strata. \*(Note: Placeholder statistical test and p-value need author confirmation.)\*

These quantitative findings strongly indicate that GoGI captures a dimension of functional importance transcending superficial characteristics like sequence length or perceived problem difficulty. This empirical evidence—demonstrating GoGI’s independence from superficial problem characteris-

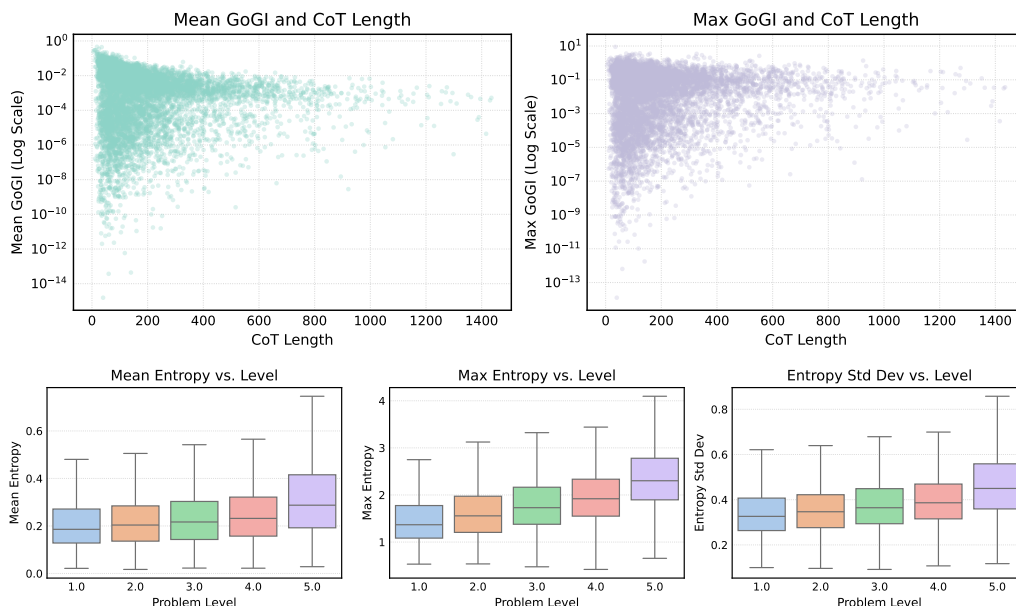


Figure 6: **Relationship between GoGI scores and external problem characteristics.** **Top:** Scatter plots showing Mean GoGI and Max GoGI score distributions versus Chain-of-Thought length. **Bottom:** Box plots showing  $\text{Log}(1 + \text{Mean GoGI})$  score distributions across MATH problem difficulty levels. The weak correlations observed suggest GoGI captures functional importance largely independent of these external characteristics.

tics—reinforces the need for dynamic, context-sensitive pruning strategies like the proposed ADS, rather than static heuristics based merely on attributes like length or perceived difficulty.

## D.2 Statistical Independence from Other Model Metrics

Next, to quantify the unique information captured by GoGI and establish its statistical relationship with other internal model metrics like predictive entropy, we computed the Spearman rank correlation matrix across various GoGI- and entropy-based statistics derived from the CoT samples (Figure 7, left).

The correlation analysis confirms several key hypotheses discussed in the main text:

**Internal Consistency** Different GoGI statistical measures exhibit high positive intercorrelations (Spearman’s  $r_s > 0.8$ ), indicating the metric’s robust internal consistency.

**Sparsity Relationship** As expected, GoGI sparsity shows a strong negative correlation with other GoGI metrics, confirming that functional importance is concentrated in relatively few tokens.

**Orthogonality to Uncertainty** Critically, correlations between core GoGI metrics and entropy-based uncertainty measures (mean, max, std. dev.) consistently show minimal association ( $|r_s|$  typically  $< 0.1$ ), providing strong quantitative evidence for their statistical independence relative to predictive entropy.

This empirical demonstration of near-orthogonality between GoGI scores and predictive uncertainty entropy ( $|r_s| < 0.1$ ) provides compelling justification for synergistically leveraging these distinct signal types within the Adaptive Dynamic Skipping (ADS) mechanism. This correlation analysis further confirms the weak associations between GoGI metrics and external characteristics noted previously (Section D.1).

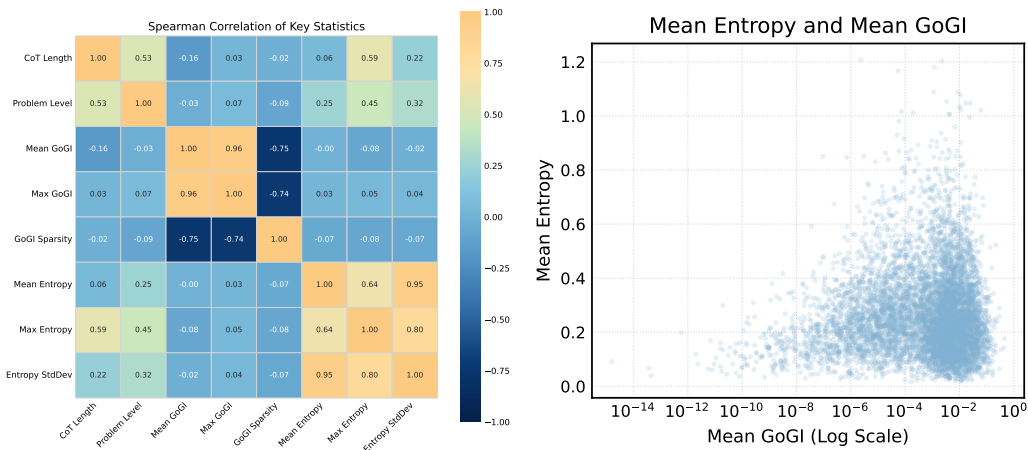


Figure 7: **Left:** Spearman rank correlation matrix quantifying relationships among key statistical measures derived from CoT samples. **Right:** Scatter plot of Mean Entropy versus Mean GoGI score per CoT sample, illustrating the lack of a clear trend and further supporting the statistical independence of these sequence-level metrics.

### D.3 Sample-Level Relationship between GoGI and Entropy

Complementing the correlation matrix, we also examined the relationship at the sequence level visually. While Figure 2 (left) indicates weak correlation at the per-token level, Figure 7 (right) confirms this independence extends to the sequence level by plotting Mean Entropy versus Mean GoGI score for each CoT sample.

The scatter plot reveals no discernible systematic relationship exists between the average functional importance of a CoT and the average predictive uncertainty during its generation. Sequences with high average importance can exhibit either high or low average uncertainty, and vice versa. This result further reinforces that GoGI and entropy capture fundamentally different aspects of the reasoning process. This finding strongly justifies their combined use within the Adaptive GoGI-Skip framework to achieve nuanced, context-aware compression.

## E Detailed Entropy Analysis

This appendix provides a comprehensive statistical analysis of predictive entropy ( $H_t$ ) observed across CoT sequences from the MATH training dataset, which the Gemma-3-4B-it model generated. Characterizing the behavior of predictive entropy ( $H_t$ ) is crucial because it functions as the primary runtime signal for uncertainty quantification within our ADS mechanism, informing both the EDR and ANC components. Figure 8 provides visual support for the analyses herein, illustrating key distributional properties and relationships with external problem attributes.

### E.1 Distributional Characteristics of Predictive Entropy

The empirical distributions for key entropy statistics, presented in the top row of Figure 8, reveal characteristic patterns. Mean Entropy typically exhibits a characteristic right-skewed distribution, with the majority of reasoning sequences demonstrating relatively low average uncertainty, however, the distribution features extended tails toward higher uncertainty regions. Maximum Entropy similarly displays right skewness but spans a considerably wider range, which confirms the occurrence of significant transient uncertainty peaks within individual reasoning sequences.

The distribution of Entropy Standard Deviation (Figure 8, top) reveals typical intra-sequence variability patterns and provides critical scaling information for the entropy mapping functions ( $\mathcal{M}, \mathcal{M}'$ ). These observed distributional characteristics directly inform the statistical normalization applied within the ADS mechanism (Sections 3.2.1 and 3.2.2). Specifically, the empirically estimated global

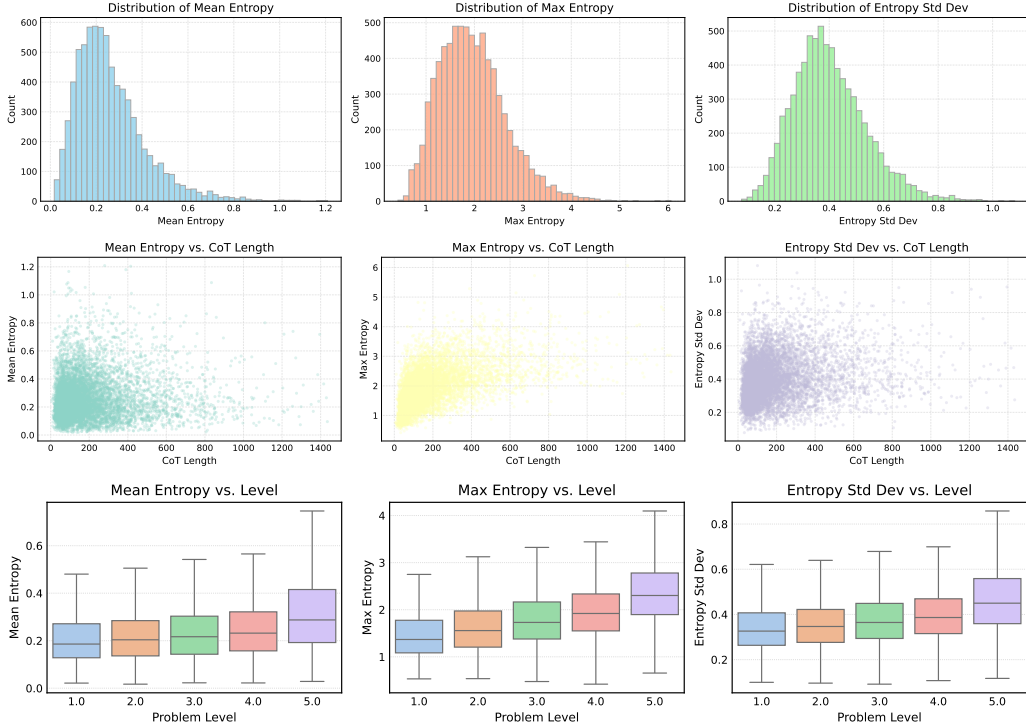


Figure 8: **Detailed statistical analysis of predictive entropy ( $H_t$ ) on the MATH dataset.** **Top:** Empirical probability distributions of Mean Entropy, Maximum Entropy, and Entropy Standard Deviation per CoT sequence, demonstrating characteristic right-skewed patterns. **Middle:** Scatter plots showing the relationship between entropy statistics and CoT sequence length, revealing minimal linear correlation between entropy metrics and sequence length. **Bottom:** Box plots illustrating the systematic variation of entropy metrics across different MATH problem difficulty levels, demonstrating a consistent positive association between entropy metrics and problem complexity.

parameters  $H_{\text{median}}$  and  $H_{\text{std}}$  are used within the mapping functions  $\mathcal{M}$  and  $\mathcal{M}'$  to standardize entropy inputs.

## E.2 Relationship Between Entropy and External Factors

The relationship between entropy statistics and CoT sequence length is examined via regression analysis (Figure 8, middle). Consistently weak linear correlations (indicated by low R-squared values for the regression lines in Figure 8, middle row) are observed across all examined entropy statistics. These minimal correlations demonstrate that sequence length alone is a poor predictor of model uncertainty patterns, this reinforces our argument that length-based compression heuristics have fundamental limitations in adapting to variable reasoning complexity.

In contrast, the relationship between entropy and problem complexity (Figure 8, bottom) is markedly different. We observe a statistically significant positive monotonic relationship between entropy metrics and MATH problem difficulty levels. Mean Entropy, Maximum Entropy, and Entropy Standard Deviation all exhibit progressively increasing trends as problem difficulty increases. This systematic relationship indicates that as problems become objectively more complex, the model generally experiences higher average uncertainty, more pronounced uncertainty peaks, and greater variability in predictive confidence during its reasoning process.

This empirically established correlation between predictive entropy and intrinsic problem complexity strongly validates using predictive entropy as a dynamic signal for modulating compression intensity in our ADS mechanism. Unlike static heuristics based on superficial characteristics, predictive entropy appears to more effectively capture the underlying cognitive demands imposed by varying task complexity, thereby enabling a more principled adaptation of the compression strategy.

## F Adaptive N-Constraint Mechanism Details

This appendix provides detailed specifications of the ANC mechanism, a critical component of Adaptive GoGI-Skip designed to preserve local coherence. We first present a quantitative analysis of its token preservation patterns and then elaborate on specific algorithmic refinements implemented in our final version.

### F.1 ANC Trigger Analysis by Token Type

The quantitative analysis summarized in Table 8 reveals distinct token preservation patterns when ANC is triggered. Although General Language Tokens account for the highest absolute number of ANC preservations due to their high frequency in the corpus, the highest \*rates\* of preservation occur for Logical Connectives (44%) and Structural Formatting elements (40%). This empirical evidence supports our hypothesis that the ANC mechanism preferentially safeguards tokens essential for structural integrity and logical coherence, even if they possess low GoGI scores.

Table 8: **Quantitative Analysis of Token Preservation by ANC Across Functional Categories.** Analysis examines 405k tokens (numbers abbreviated with 'k' for thousands) from the MATH test set processed by Gemma-3-4B-it. *Initially Pruned* refers to tokens with  $G'_t < \tau_t$ . *Preserved by ANC* identifies tokens that would have been pruned based on GoGI scores alone but were retained due to the N-constraint. *ANC Preservation Rate* represents the percentage of initially pruned tokens ultimately preserved by the mechanism.

Functional Category	Total Count	Initially Pruned	Preserved by ANC	Preservation Rate
Mathematical Numerals	50k	5.3k	1.5k	30%
Mathematical Operators	40k	5.7k	2.1k	33%
Mathematical Symbols	30k	4.5k	1.3k	29%
Structural Formatting	60k	24.0k	9.6k	40%
Logical Connectives	25k	11.0k	4.8k	44%
General Language Tokens	200k	130.0k	39.0k	30%
<b>Aggregate Statistics</b>	405k	180.5k	58.3k	32%

The substantial preservation rates observed for mathematical elements (Numerals, Operators, Symbols, averaging approx. 30-33%) further demonstrate ANC’s effectiveness in preventing the fragmentation of essential calculation sequences, particularly when intermediate mathematical tokens exhibit low GoGI scores in isolation. This analysis confirms that ANC acts as a crucial coherence-preserving complement to the primary goal-oriented pruning mechanisms (GoGI, EDR), maintaining structural elements that purely importance-driven filtering might otherwise erroneously discard.

### F.2 Algorithmic Refinements

The core Adaptive GoGI-Skip pruning algorithm (Section 3.3) integrates GoGI, EDR, and ANC. To enhance the algorithm’s robustness and responsiveness—particularly concerning the ANC component—the specific implementation used to generate our main results incorporates several refinements to the core logic:

**Entropy Gradient Detection** We monitor the change in normalized entropy,  $\Delta \hat{H}_t = \hat{H}_t - \hat{H}_{t-1}$ , between consecutive tokens. If the magnitude  $|\Delta \hat{H}_t|$  exceeds a high threshold  $\delta_{high}$  (set to 0.3 based on preliminary tuning), indicating a sharp transition in uncertainty, we temporarily reduce the adaptive N-constraint  $N_t$  for the current step (by multiplying it by 0.8, subject to  $N_{min}$ ) to enforce stricter coherence during potential reasoning shifts. Conversely, if  $|\Delta \hat{H}_t|$  remains below a low threshold  $\delta_{low}$  (set to 0.05) for a defined period (e.g., 3 consecutive steps, indicating stability), we might temporarily increase  $N_t$  (subject to  $N_{max}$ ) to allow more aggressive pruning during potentially redundant phases.

**Compression Rate Modulation of N** The calculated  $N_t$  value is further modulated based on the overall target compression ratio ( $\gamma_{target}$ , set manually or estimated by the Adaptive Parameter Tuner). More aggressive target compression (lower  $\gamma_{target}$ ) increases the effective  $N_t$  applied (via a scaling factor  $s_N > 1$ , potentially defined as  $s_N = 1 + k \cdot (0.5 - \gamma_{target})$  for  $\gamma_{target} < 0.5$ , where  $k$  is

a sensitivity hyperparameter), while more conservative targets decrease it (scaling factor  $s_N < 1$ ). \*(Note: Specific scaling function needs author confirmation/replacement.)\* This tuning aligns the local coherence constraint with the global efficiency objective.

**Extreme Low-Importance Override** To prevent the N-constraint from preserving genuinely irrelevant low-importance tokens, we implement an override rule. If a token’s weighted GoGI score  $\mathcal{G}'_t$  falls below a fixed critical fraction (hyperparameter  $\theta_{critical} = 0.4$ ) of the dynamic threshold  $\tau_t$ , we prune the token irrespective of the consecutive skip count  $C_{t-1}$  and the current N-constraint  $N_t$ .

**Boundary Condition Management** To ensure robust entropy estimation near sequence boundaries when calculating the windowed average  $\bar{H}_{t,W}$  (Eq. 7), we employ edge-value padding.

We found in preliminary experiments that these refinements collectively improve the stability and effectiveness of the dynamic pruning process. Consequently, this refined algorithm was used for generating the final compressed dataset employed for training the Adaptive GoGI-Skip models reported in the main paper (Tables 1 and 2).

## G Quantitative Validation of Dynamic Compression Mechanisms

This appendix provides an in-depth quantitative analysis of the multi-factor dynamic compression behavior produced by our ADS mechanism, using the visualization presented in Figure 2 (right panel). This visualization plots the effective token retention rate ( $1 - \text{compression ratio}$ ) as a function of normalized runtime entropy and normalized CoT length. Crucially, the analysis is stratified across different global GoGI score distribution profiles, represented by panels corresponding to varying levels of importance concentration.

### G.1 Analysis of Multi-dimensional Compression Dynamics

The visualization (Figure 2, right) reveals critical insights into the complex interplay between GoGI context, entropy, and sequence length in governing the dynamic pruning decisions made by the ADS mechanism. We analyze the influence of each major factor below:

**Entropy-Driven Regulation** Focusing on the influence of entropy, the visualization demonstrates a clear positive association between normalized entropy (uncertainty) and the calculated token retention rate ( $\gamma_t$ ). As entropy increases along the vertical axis, the surface plot exhibits consistently brighter coloration (higher retention rate) and higher elevation, which indicates more conservative pruning under conditions of heightened uncertainty. This observation visually confirms the fundamental principle of EDR regulation: the framework adaptively preserves more content when facing greater predictive uncertainty. Notably, the non-linear nature of this response reflects the specific mapping function  $\mathcal{M}$  employed (see Appendix A).

**Length-Sensitivity Analysis** Second, the influence of normalized CoT length appears more nuanced. While increasing length sometimes correlates with modestly decreased retention rates (visualized as darker coloration or lower elevation), suggesting longer sequences may offer slightly greater compression opportunities, this trend is not uniform and its magnitude varies considerably across different entropy and importance regimes.

**GoGI Distribution Effects** Finally, comparing across the panels illustrates the foundational influence of the importance distribution. Higher GoGI concentration levels consistently yield higher baseline retention rates across the entropy/length space. This systematic progression confirms that the global GoGI profile establishes the overall importance context, which local predictive entropy then dynamically modulates via the EDR mechanism.

### G.2 Integrated Interpretation

This analysis of the visualization in Figure 2 (right) empirically validates that the resulting compression strategy emerges from the synergistic integration of multiple complementary signals:

- Token-specific functional importance (determined by GoGI score  $\mathcal{G}'_t$ ).

- Real-time model uncertainty (measured by predictive entropy  $H_t$ ).
- Broader sequence context (partially captured by factors like normalized length and potentially windowed entropy  $\bar{H}_{t,W}$  used in ANC, though ANC’s direct effect isn’t plotted here).

This multi-dimensional adaptive framework thus enables nuanced compression decisions that dynamically balance efficiency objectives against the preservation of functionally critical information across diverse reasoning contexts. The observed parameter interactions visually substantiate our theoretical model of adaptive compression integrating these diverse signals. This provides further visual and quantitative evidence supporting the superiority of such dynamic approaches over static strategies incapable of accommodating such contextual variation.

## H Qualitative Case Studies of CoT Compression Methods

This appendix presents a qualitative analysis comparing how different strategies compress Chain-of-Thought (CoT) reasoning sequences. We use a representative example from the MATH dataset to elucidate the distinctive operational characteristics of Adaptive GoGI-Skip relative to several baseline methods. This analysis complements the quantitative evaluations (Section 4) by providing concrete illustrations of compression behavior.

### H.1 Case Study: MATH Training Sample

#### Problem

The sequence of integers in the row of squares and in each of the two columns of squares form three distinct arithmetic sequences. What is the value of  $N$ ?

```

\draw((0,0)--(7,0)--(7,1)--(0,1)--cycle);\draw((1,0)--(1,1));
\draw((2,0)--(2,1));\draw((3,0)--(3,1));\draw((4,0)--(4,1));
\draw((5,0)--(5,1));\draw((6,0)--(6,1));
\draw((6,2)--(7,2)--(7,-4)--(6,-4)--cycle);\draw((6,-1)--(7,-1));
\draw((6,-2)--(7,-2));\draw((6,-3)--(7,-3));\
ndraw((3,0)--(4,0)--(4,-3)--(3,-3)--cycle);\draw((3,-1)--(4,-1));
\draw((3,-2)--(4,-2));\nlabel{"21", (0.5,0.8),S);
\nlabel{"14", (3.5,-1.2),S);\nlabel{"18", (3.5,-2.2),S);
\nlabel{"N", (6.5,1.8),S);\nlabel{"-17", (6.5,-3.2),S);\n[/asy]

```

#### Original CoT (count: 156)

Since  $18 - 14 = 4$ , the common difference in the first column of squares is 4, so the number above 14 is  $14 - 4 = 10$ , and the number above 10 is  $10 - 4 = 6$ . This is also the fourth number in the row, so the common difference in the row is  $(6 - 21)/3 = -5$ . Then the seventh (and last) number in the row is  $21 - 5 \cdot 6 = -9$ . In the second column, the common difference is  $[(-17) - (-9)]/4 = -2$ , so  $N = -9 - (-2) =$

#### Prompting Baseline (count: 118)

The common difference for the first column is 4 (18-14). The number above 14 is 10 (14-4), and above that is 6 (10-4). This is the 4th number in the row. The common difference for the row is -5 ((6-21)/3). The 7th number is -9 (21 - 5\*6). The difference for the second column is -2 ((-17 - -9)/4). Therefore,  $N = -9 - (-2) =$

### C3ot Baseline (count: 106)

The common difference in the first column is  $18 - 14 = 4$ . The number above 14 is  $14 - 4 = 10$ , above 10 is  $10 - 4 = 6$ . This is the fourth number in the row. The common difference in the row is  $(6 - 21)/3 = -5$ . The seventh number is  $21 - 5 \cdot 6 = -9$ . In the second column, the difference is  $[(-17) - (-9)]/4 = -2$ . So  $N = -9 - (-2) =$

### Spiritft Baseline (count: 109)

Since  $18 - 14 = 4$ , common difference first column 4, number above 14 is  $14 - 4 = 10$ , number above 10 is  $10 - 4 = 6$ . This is fourth number in row, common difference row is  $(6 - 21)/3 = -5$ . Then seventh last number row  $21 - 5 \cdot 6 = -9$ . In second column, common difference  $[(-17) - (-9)]/4 = -2$ , so  $N = -9 - (-2) =$

### TokenSkip 0.5 Baseline (count: 105)

$18 - 14 = 4$  common difference first column 4 above 14  $14 - 4 = 10$   
above 10  $10 - 4 = 6$  fourth number row common difference  $(6 - 21)/3$   
 $= -5$  seventh last  $21 - 5 \cdot 6 = -9$  second column difference  
 $[(-17) - (-9)]/4 = -2$   $N = -9 - (-2) =$

### Adaptive GoGI-Skip (count: 87)

$18 - 14 = 4$  in squares 4 so 14  $14 - 4 = 10$  above  $10 - 4 = 6$ . fourth so row  
 $(6 - 21)/3 = -5$ . seventh and the is  $21 - 5 \cdot 6 = -9$ . the is  
 $[(-17) - (-9)]/4 = -2$ , so  $N = -9 - (-2) =$

## H.2 Comparative Analysis of Compression Strategies

Based on the examples above, this comparative analysis highlights the distinct operational characteristics of the evaluated compression approaches:

**Original CoT (156 tokens)** Provides a complete, syntactically coherent explanation featuring explicit verbal connectors such as "Since", "so", "Then", and "In" between computational steps and thorough elaborations of the mathematical reasoning principles involved.

**Prompting Baseline (118 tokens)** Retains most semantic content but uses more concise phrasing (omitting phrases like "squares is 4, so the number above 14 is") and introduces parenthetical notation for calculations, such as '(18-14)'. This achieves moderate compression (24% token reduction) with only minor structural modification compared to the original CoT structure.

**C3ot Baseline (106 tokens)** Systematically removes select function words like "is" and redundant explanatory phrases such as "of squares is 4, so the number above 14 is" while preserving core mathematical notation and sentence structure. This results in 32% token reduction with minimal grammatical disruption.

**SpiritFT Baseline (109 tokens)** Applies a more aggressive reduction of linguistic elements, removing items like the leading "Since", articles, and some auxiliary verbs while maintaining critical mathematical expressions and basic sentence structure, achieving 30% token reduction.

**TokenSkip ( $\gamma \approx 0.5$ , 105 tokens)** Reduces explanatory language significantly, yielding primarily keyword/numerical sequences like "18 - 14 = 4 common difference first column 4". It strongly prioritizes preserving mathematical operators and numerical relationships, achieving 33% token reduction.

**Adaptive GoGI-Skip (87 tokens)** Achieves maximal efficiency in this comparison (44% token reduction) via precise identification and prioritization of functionally critical tokens. It systematically preserves essential numerical expressions and calculations, including  $18 - 14 = 4$ ,  $14 - 4 = 10$ , and  $(6 - 21)/3 = -5$ , while aggressively pruning descriptive language elements like the phrases "common difference" and "number above", connectives such as "so", and articles like "the", and even some spacing elements deemed non-contributory to the final calculation's accuracy.

This comparative analysis highlights how Adaptive GoGI-Skip's goal-oriented importance scoring facilitates uniquely effective identification and preservation of mathematically essential tokens. This results in the most efficient compression among the evaluated methods while preserving the integrity of the solution steps. In contrast to static approaches applying uniform compression patterns, Adaptive GoGI-Skip's adaptive modulation of pruning intensity based on localized functional relevance demonstrates a superior capacity for contextually-aware compression.